Published in final edited form as:
Invest Ophthalmol Vis Sci. 2009 February ; 50(2): 717–728. doi:10.1167/iovs.08-2321.

TRPV1: Contribution to Retinal Ganglion Cell Apoptosis and Increased Intracellular Ca^{2+} with Exposure to Hydrostatic Pressure

Rebecca M. Sappington, **Tatiana Sidorova**, **Daniel J. Long**, and **David J. Calkins**
Vanderbilt Eye Institute, Vanderbilt University Medical Center, Nashville, Tennessee

Abstract

Purpose—Elevated hydrostatic pressure induces retinal ganglion cell (RGC) apoptosis in culture. The authors investigated whether the transient receptor potential vanilloid 1 (TRPV1) channel, which contributes to pressure sensing and Ca^{2+}-dependent cell death in other systems, also contributes to pressure-induced RGC death and whether this contribution involves Ca^{2+}.

Methods—*trpv1* mRNA expression in RGCs was probed with the use of PCR and TRPV1 protein localization through immunocytochemistry. Subunit-specific antagonism (iodo-resiniferatoxin) and agonism (capsaicin) were used to probe how TRPV1 activation affects the survival of isolated RGCs at ambient and elevated hydrostatic pressure (+70 mm Hg). Finally, for RGCs under pressure, the authors tested whether EGTA chelation of Ca^{2+} improves survival and whether, with the Ca^{2+} dye Fluo-4 AM, TRPV1 contributes to increased intracellular Ca^{2+}.

Results—RGCs express *trpv1* mRNA, with robust TRPV1 protein localization to the cell body and axon. For isolated RGCs under pressure, TRPV1 antagonism increased cell density and reduced apoptosis to ambient levels ($P \leq 0.05$), whereas for RGCs at ambient pressure, TRPV1 agonism reduced density and increased apoptosis to levels for elevated pressure ($P \leq 0.01$). Chelation of extracellular Ca^{2+} reduced RGC apoptosis at elevated pressure by nearly twofold ($P \leq 0.01$). Exposure to elevated hydrostatic pressure induced a fourfold increase in RGC intracellular Ca^{2+} that was reduced by half with TRPV1 antagonism. Finally, in the DBA/2 mouse model of glaucoma, levels of TRPV1 in RGCs increased with elevated IOP.

Conclusions—RGC apoptosis induced by elevated hydrostatic pressure arises substantially through TRPV1, likely through the influx of extracellular Ca^{2+}.

Throughout the central nervous system, pressure is a highly relevant and potent stimulus. This is so especially in sensory function and in sympathetic systems, in which various membrane-bound receptors play an important role in transducing pressure to neural signals.[1–7] Elevated intraocular pressure (IOP) is a leading risk factor for the degeneration of retinal ganglion cells (RGCs) and their axons during traumatic injury and in chronic disease, particularly glaucoma.[8–11] However, the mechanisms through which pressure translates to RGC death are not known. To probe these mechanisms, model systems making use of hydrostatic pressure as a stressor for isolated RGCs plated on a rigid surface and exposed to a liquid column are useful. Although these systems do not replicate IOP, the retinochoroidal complex experiences hydrostatic pressure from within the vitreal chamber and from the

Corresponding author: David J. Calkins, Department of Ophthalmology and Visual Sciences, The Vanderbilt Eye Institute, Vanderbilt University Medical Center, Ophthalmology Research Lab, 1105 Medical Research Building IV, Nashville, TN 37232-0654; david.j.calkins@vanderbilt.edu.

Disclosure: **R.M. Sappington**, P; **T. Sidorova**, P; **D.J. Long**, P; **D.J. Calkins**, P

suprachoroidal space; its gradient is IOP dependent.[12,13] Similarly, RGC axons in the optic nerve are exposed continuously to hydrostatic pressure from cerebrospinal fluid.[13] It is well established that RGCs exposed to elevated hydrostatic pressure in vitro undergo cellular apoptosis, even in the absence of the multitude of other factors associated with elevated IOP (e.g., glial activation, ischemia). Pressure-induced RGC apoptosis in vitro depends on the magnitude of pressure exposure, correlates with the upregulation of a variety of apoptotic and early-immediate genes, and involves oxidative stress.[14–18] These events are similar to those in common animal models of glaucoma,[19–25] and this similarity bolsters the use of hydrostatic pressure as a stimulus for probing the RGC response to pressure.

Members of the transient receptor potential (TRP) family of cation-selective ion channels have long been implicated in mechanical and tactile sensitivity.[26–34] Like other TRP subunits, activation of the capsaicin-sensitive vanilloid subunit 1 (TRPV1) is associated with a variety of stimuli.[35] TRPV1 in sensory ganglia of the spinal cord and in the peripheral nervous system responds to mechanical stimuli involved in several systemic functions, including pressure-induced pain, injury monitoring, and visceral distension.[36–48] In addition, like other TRP subunits, TRPV1 activation is associated with a robust Ca^{2+} conductance that has been linked to apoptotic cell death, including that of neurons and glia.[49–52] Similarly, we recently demonstrated that TRPV1 expressed by retinal microglia contributes to a Ca^{2+}-dependent signal involved in nuclear translocation of NFκB and the release of the inflammatory cytokine IL-6 with exposure to hydrostatic pressure in vitro.[53] Thus, it is reasonable to ask whether RGCs similarly express TRPV1 and whether this expression could contribute to the apoptosis associated with exposure to elevated hydrostatic pressure. Here we demonstrate that TRPV1 expressed by RGCs contributes to pressure-induced apoptosis and that the TRPV1-initiated cascade involves the influx of Ca^{2+}, as in other cell types.[49–53]

Materials and Methods

Animals and Tissue Preparation

This study was conducted in accordance with regulations set forth in the ARVO Statement for the Use of Animals in Ophthalmic and Vision Research. Animal protocols were approved by the Institutional Animal Care and Use Committee of Vanderbilt University Medical Center. For histology, adult Sprague-Dawley rats (Charles River Laboratories, Wilmington, MA) were perfused with 4% paraformaldehyde (Sigma, St. Louis, MO), their eyes were enucleated, and the retina was removed for wholemount preparations or embedded in paraffin for cross-sections (6-μm thick). Paraformaldehyde (4%)-fixed whole eyes from 6- and 9-month-old DBA/2 mice with lower IOP (average: 14.85 mm Hg for 6 months, 18.5 mm Hg for 9 months) or higher IOP (average: 17.7 mm Hg for 6 months, 21.8 mm Hg for 9 months) were obtained from The Jackson Laboratory (Bar Harbor, ME). As previously described, IOP was measured (Tono-Pen; Reichert) before euthanatization.[54] For comparison, whole eyes were also obtained from adult C57/BL6 mice (The Jackson Laboratory). These eyes were embedded in paraffin and cross-sectioned at 6 μm. For RNA, whole retinas from adult Sprague-Dawley rats (Charles River Laboratories) were obtained fresh and flash frozen on dry ice. For isolation of adult RGCs, eyes from 3-month-old Sprague-Dawley rats (Charles River Laboratories) were enucleated, and their retinas were removed. RGCs were isolated by immunomagnetic separation.[18] For primary cultures of purified RGCs, eyes from postnatal day (P) 4 to P10 Sprague-Dawley rats were enucleated, their retinas were removed, and RGCs were isolated by immunomagnetic separation.[18]

The use of postnatal retina for purification of RGCs is well documented by our laboratory[18] and others.[16,55–61] The P4–P10 developmental stage is particularly advantageous for the isolation of RGCs because the apoptotic elimination of excess RGCs during development is

complete, and the remaining RGCs have a functional axon in the optic nerve with arborization of presynaptic terminals within the brain.[62–64] Furthermore, the relatively undifferentiated state of other neurons in the retina eases dissociation of the retina and specificity of antigen-based isolation.[62,63]

Cell Separation and Primary Culture

Primary cultures of purified RGCs were prepared as previously described.[18] Briefly, RGCs were harvested by immunomagnetic separation with the use of mouse anti–rat Thy-1.1/CD90 IgG (5 μg/mL; BD PharMingen, San Diego, CA) and metallic microbeads conjugated with anti–mouse IgG. Microglia were depleted before isolation of RGCs using mouse anti–rat RT1a/OX18 IgG (5 μg/mL; catalog number CBL1519; Chemicon/Millipore, Billerica, MA) followed by incubation with anti–mouse IgG microbeads. RGCs were plated at a density of approximately 3×10^3 cells in each well of eight-chamber glass slides (Labtek 2; Nal-Nunc, Rochester, NY) coated with laminin (0.01 mg/mL; Sigma) and poly-$_D$-lysine (0.01 mg/mL; Sigma) and were grown in serum-free, B27-supplemented media (NeuroBasal; Gibco, Carlsbad, CA) containing 2 mM glutamine, 0.1% genomycin, 1% NB_{2B} supplement (500 μg/mL insulin, 10 mg/mL transferrin, 630 ng/mL progesterone, 1.6 mg/mL putrescine, and 520 ng/mL selenite; Gibco), 50 ng/mL brain-derived nerve growth factor (Invitrogen, Carlsbad, CA), 20 ng/mL ciliary neurotrophic factor (Invitrogen), 10 ng/mL basic fibroblast growth factor (Invitrogen), and 100 μM inosine (Sigma). Cells were used for experiments 4 days after plating. As previously described,[16] we assessed the purity of all preparations with PCR and immunocytochemistry against cell type-specific markers to exclude contaminating cell types, including Müller glia (cyclin D3), astrocytes (GFAP), and microglia (CD68 and OX18). Samples from all RGC preparations demonstrated strong immunolabeling for Thy-1.1 in approximately 95% of cells with normal-appearing nuclei.

RGCs were isolated from adult retina using the same protocol for immunomagnetic separation used for postnatal RGCs with the addition of hyaluronidase (10 U/μL) to papain-mediated dissociation of the retina. Isolation of adult RGCs also required the addition of DNaseI (0.005%; Invitrogen) to centrifugation cycles. Unlike postnatal RGCs, adult RGCs were immediately placed in lysis buffer for RNA extraction.

Reverse Transcription Polymerase Chain Reaction

Total RNA was extracted from isolated RGCs, RGC cultures, and whole retina with the use of extraction kits (MicroRNA and RNeasy; Qiagen, Inc., Valencia, CA), according to manufacturer's instructions. RT-PCR was performed as previously described.[18,65] After first- and second-strand synthesis of cDNA, gene-specific PCR was conducted for 30 cycles with the primers (Integrated DNA Technologies, Coralville, IA) mouse *actin* (5′-TCC TGG GTA TGG AAT CCT GTG G-3′; 5′-CTT GAG TCA AAA GCG CCA AAA C-3′) and rat *trpv1* (5′-CAA GCA CTC GAG ATA GAC ATG CCA-3′; 5′ -ACA TCT CAA TTC CCA CAC ACC TCC-3′. Actin was used to confirm the presence of comparable cDNA concentrations between samples. To ensure that genomic DNA was not the source of PCR products, primers for *actin* and *trpv1* were designed to span an intron. In addition, gene-specific PCR was performed on an aliquot of each sample that did not undergo reverse transcription. PCR products of 514 bp (*actin*) and 282 bp (*trpv1*) were separated on an agarose gel stained with ethidium bromide and digitally imaged on a gel reader (Alpha Innotech, San Leandro, CA).

Riboprobe Synthesis and In Situ Hybridization

A fragment corresponding to 206 bp to 658 bp of *trpv1* was isolated (primers CCTATCATCACCGTCAGCTCTGT and GGCAATGTGTAATGCT GTCTGG) from a plasmid containing the full-length sequence of rat *trpv1* (a generous gift from David Julius,

University of California at San Francisco, San Francisco CA) and subcloned into pCR2.1 vector (Invitrogen). After sequencing and linearization, sense (T3: AATTAACCCTCACTAAAGGGCAAGCACTCGAGATA GACATGCCA) and antisense (T7: TAATACGACTCACTATAGGGACATCTCAA TTCCCACACACCTCC) riboprobes were transcribed and DIG labeled (Boehringer Mannheim, Mannheim, Germany). For in situ hybridization, paraffin sections of retina from adult rat were deparaffinized in xylene, rehydrated, and postfixed in 4% paraformaldehyde. After treatment with acetic anhydride and proteinase K, tissue was dehydrated and incubated with sense or antisense DIG-labeled riboprobe against rat *trpv1* (10 pg/μL) in hybridization buffer (DakoCytomation, Glostrup, Denmark). DIG label was detected with an alkaline phosphatase-conjugated anti–DIG antibody (1:500; Roche) and visualized with 1.5 mg/mL nitroblue tetrazolium (NBT; Roche) and 750 μg/mL 5-bromo-5-chloro-3-indolyl phosphate (BCIP; Roche) in 100 mM Tris-HCl, pH 9.5, 100 mM NaCl.

Hydrostatic Pressure Experiments

Primary cultures of purified RGCs and whole retina explants were maintained at ambient pressure in a standard incubator or at +70 mm Hg hydrostatic pressure using a custom-made regulator chamber placed in the incubator, as described previously in detail.[16,18,53,65] Briefly, a humidified pressure chamber equipped with a regulator and a gauge was placed in a 37°C incubator, and a mixture of 95% air and 5% CO_2 was pumped into the chamber to obtain +70 mm Hg pressure (9% increase above atmospheric pressure) that was maintained by the regulator. We chose this pressure setting for direct comparison with our previous studies and those of others.[14–18,53,65] For ambient pressure experiments, cells were kept in a standard incubator. As previously described, others and we have experimentally ruled out significant artifacts caused by changes in pH, dissolved oxygen content, dissolved carbon dioxide content, and culture nutrition.[16,53,65]

Pharmacology

For TRPV1-specific antagonism, we used iodo-resiniferatoxin (I-RTX; Alexis Biochemicals, Lausen, Switzerland). The specific action of I-RTX on TRPV1 has been well vetted in the TRP pharmacology literature, including its use in heterologous expression systems and a demonstrated affinity for TRPV1 800-fold higher than the synthetic capsaicin analog, capsezepine.[53,66–70] Of note, I-RTX completely eradicates capsaicin-induced currents in cells heterologously expressing rat or human TRPV1.[66–70] For TRPV1-specific agonism, we again used a widely accepted TRPV1-specific agent capsaicin (Sigma).[71–73] Stock solutions of pharmacologic agents were diluted with RGC culture media to produce the following final concentrations: 100 nM, 10 nM, 1 nM, or 100 pM for I-RTX; 100 μM, 10 μM, or 1 μM for capsaicin; and 950 μM ethylene glycol-bis(B-aminoethyl)-N,N,N^1,N^1-tetraacetic acid (EGTA; Gibco).[74] The 950-μM dose of EGTA reduced the concentration of available Ca^{2+} in the culture media from 1 mM to 100 μM, as determined by Max Chelator (Stanford University, Stanford, CA). Stock solutions were prepared with 10 mM I-RTX in dimethyl sulfoxide, 10 mM capsaicin in ethanol, 100 mM EGTA in NaOH-buffered ddH_2O. Control cultures for pharmacology studies were treated with an equivalent volume of the appropriate vehicle. Cultures treated with EGTA or I-RTX were used in 48-hour hydrostatic pressure experiments. Cultures treated with capsaicin or its vehicle were maintained at ambient pressure in a standard incubator for 48 hours.

In Situ Apoptosis Assay and Quantification

As previously described, we assessed apoptosis of RGCs using a terminal deoxynucleotidyl transferase-mediated dUTP nick-end labeling (TUNEL; Serologicals/Millipore) assay with DAPI counterstain (Molecular Probes, Eugene, OR).[18] For quantification of RGC apoptosis in purified cultures, we photographed 10 random fields in each well of the culture plate to

obtain a minimum of 30 fields for each experimental condition. Cell density was determined by counting the number of DAPI-stained nuclei per square millimeter. TUNEL reactivity was assessed as the percentage of DAPI-stained cells that were TUNEL positive.[18] For TUNEL imaging, an automated macro was used for image analysis to reduce subjectivity and bias. As previously described, the quantification macro for TUNEL labeling was developed using Image Pro Plus (version 5.1.2; Media Cybernetics, San Diego, CA).[18] For analysis of TUNEL images, the automated macro applied filters to set the intensity range and to discriminate roundness and size. Objects that met the predetermined parameters for label intensity, nuclei shape, and nuclei size were then counted as TUNEL-positive cells.

Western Blot

Western blot analysis was conducted as previously described with some modification.[75] Protein lysates were produced from retina homogenized (1 retina/100 μL) in solution containing 50 mM Tris, pH 6.8, 2% SDS, 10% glycerol, 100 mM dithiothreitol, 2 mM EDTA, 50 mM NaF, 0.2 mM Na_3VO_4, 0.25 mM phenylmethylsulfonyl fluoride, and protease inhibitor cocktail (Roche). Protein concentration was determined with protein assay (Bio-Rad, Hercules, CA). Samples (60–80 μg protein) were prepared in denaturing buffer containing 100 mM Tris-HCl, pH 6.8, 4% SDS, 20% glycerol, 0.2% bromophenol blue, and 200 mM dithiothreitol. Samples were then separated by SDS-PAGE in 4% to 20% gradient Tris-glycine precast gel (Bio-Rad) and transferred to a membrane (Millipore). The membrane was incubated for 1 hour in blocking solution containing 5% powdered milk and 0.05% Tween-20, pH 7.6. This was followed by overnight incubation at 4°C in primary antibody. For rat tissue, we used rabbit anti–rat TRPV1 IgG (1:1000; catalog number NB100–1617; Novus Biologicals, Littleton, CO) against amino acids 4 to 20 (RASLDSEESESPPQENSC) in the *n* terminus of rat TRPV1. In Western blot, this antibody recognizes full-length TRPV1, in any glycosylation state, with a product size of 100 to 113 kDa and a dimer at 198 kDa; its specificity for immunoblotting and labeling in neural tissue has been established.[76–78] For mouse tissue, we used rabbit anti–mouse TRPV1 IgG (1:500; catalog number RA14113; Neuromics, Edina, MN) against the absolute C terminus of mouse TRPV1 (EDAEVFKDSMAPGEK). In Western blot, this antibody yields a product of 90 to 113 kDa for full-length TRPV1 of varying glycosylation states and of 198 kDa for TRPV1 dimers. The specificity of this antibody has been established by immunoblotting and labeling in expression systems and mouse neural tissue, including the most commonly used $trpv1^{-/-}$ mouse, which yielded no reactivity.[79–81] As a loading and reaction control, we also probed all samples with mouse anti–β-actin IgG (1.2 μg/mL; Ambion, Foster City, CA). The expected molecular weight of B-actin is 42 kDa. For neutralization of TRPV1, the anti–rat TRPV1 antibody was preincubated with blocking peptide (20 μg/mL; Novus Biologicals) for 4 hours at room temperature before overnight incubation. After washes in blocking solution, membranes were incubated for 1 hour in blocking solution containing goat anti–rabbit IgG (400 ng/mL; Molecular Probes) or mouse anti– rabbit IgG (400 ng/mL; Molecular Probes) conjugated to Alexa Fluor 680. After washes in PBS + 20% Tween, immunoreactive bands were detected by an infrared imaging system (Odyssey; Li-Cor, Lincoln, NE).

Immunohistochemistry

Immunolabeling in primary cultures of RGCs, vertical sections of retina, and wholemounts of retina was performed with slight modification as previously described.[18,65,75,82] Immunolabeling was performed with the TRPV1 antibodies described (for rat, 1:100; for mouse, 1:50), mouse anti–SMI32 (1:10,000; catalog number SMI-32R; Covance, Berkeley, CA), and mouse anti–rat Thy-1.1/CD90 IgG (5 μg/mL; BD PharMingen) and was visualized with goat anti–mouse IgG or goat anti–rabbit IgG conjugated with Alexa 594 or 488 dye (10 μg/mL; Molecular Probes). Some samples were also counterstained with DAPI (50 μg/mL; Molecular Probes). Controls for immunohistochemistry experiments were conducted with

no primary antibody and the appropriate IgG isotypes. RGC cultures and vertical sections of retina were imaged on an upright microscope (AX70; Olympus, Melville, NY), whereas wholemount preparations of retina were imaged on the upright confocal microscope (LSM5 META; Zeiss, Thornwood, NY).

Fluorescence Microscopy and Quantification

Unless otherwise stated, all microscopy was performed on an upright microscope (AX70; Olympus) equipped with four fluorescent cubes, Nomarski-DIC optics, and a semicooled CCD camera (Spot RT; Diagnostic Instruments, Sterling Heights, MI). Digital images were acquired with acquisition software (Spot Image; Diagnostic Instruments).

Confocal Microscopy

Imaging of immunohistochemistry was performed at the Vanderbilt Cell Imaging Core on an upright confocal microscope (LSM510 META; Zeiss) equipped with laser scanning fluorescence (blue/green, green/red, red/far-red) and Nomarski-DIC, 3-D z-series, and time series. All samples were examined with a 63× oil-immersion objective (1.40 Plan-apochromat), and images were acquired with a digital camera and image analysis software (LSM5; Zeiss).

Calcium Signaling Experiments

To assess pressure-induced changes in intracellular Ca^{2+}, we used Ca^{2+} dye (Fluo-4 AM; Molecular Probes), as described in our recent study of microglial cells.[53] Briefly, the Ca^{2+} dye (Fluo-4 AM; Molecular Probes) is a BAPTA-based, high-affinity, nonratiometric Ca^{2+} dye known to exhibit greater than a 40-fold increase in fluorescence on Ca^{2+} binding.[83] Because we are interested in longer changes in intracellular Ca^{2+} that could lead to cell death, we examined Fluo-4 label after exposure to pressure for 1 hour. This is consistent with the period for reliable detection and interpretation of Fluo-4 label.[83] To allow complete de-esterification of Fluo-4 AM, primary RGC cultures were loaded with 5 μM Fluo-4 AM for 30 minutes in a standard culture incubator. The media were replaced, and the cultures were examined to confirm comparable Fluo-4 loading. When this was complete, the cultures were segregated into control and experimental groups. The experimental group was exposed to +70 mm Hg hydrostatic pressure for 1 hour, and the control group was maintained in a standard culture incubator. The use of separate cultures for measurement of Fluo-4 label at ambient and elevated pressure implies that no internal control is present for initial dye loading or dye leakage over time. We attempted to minimize these effects by examining each culture for equivalent dye loading and excluding any culture that was not equivalently loaded before the experimental period. We used three to six culture plates per condition, for which the mean Fluo-4 intensity was determined and used in statistical comparisons. Thus, a bias in dye loading would have to occur simultaneously in as many as six cultures. Immediately after the experiment, the live cultures were coverslipped with physiological saline and imaged as detailed. For each sample, 15 to 20 independent fields (20×) were acquired, surface plots were created, and Fluo-4 intensity was quantified as total fluorescent intensity across the field. Ca^{2+} imaging was performed on the upright microscope (AX70; Olympus).

Experimental Design and Statistical Analysis

All preparations, experiments, and measurements were performed minimally in triplicate, with Student's *t*-test as an indicator of significance unless stated otherwise.

Results

TRPV1 Expression in RGCs of the Rat Retina

A PCR investigation revealed that expression of *trpv1* mRNA in isolated adult and postnatal RGCs was significantly lower than that of whole retina (Fig. 1A). This is likely attributable to the expression of *trpv1* by cell types other than RGCs in whole retina, as we have shown.[53] For isolated RGCs, the level of *trpv1* expression was similar in RGCs isolated from adult and postnatal retina. However, expression of *trpv1* by postnatal RGCs increased slightly with time in culture (Fig. 1A, right). Although a sense MRNA probe against *trpv1* produced no label as a control (Fig. 1B), an antisense probe revealed strong expression in the middle tier of the inner nuclear layer of the rat retina, probably in cell bodies of Müller glia and microglia based on their size and location (Fig. 1B). Prominent label also distributed densely throughout the large cell bodies of RGCs and in smaller cell bodies below them (Figs. 1B, 1C). Based on our previous study,[53] the latter are likely to at least include microglia cells.

In cross-sections through rat retina, immunolabeling for TRPV1 was apparent in processes penetrating the outer plexiform layer, probably from Müller glia cells, microglial cells, or both (Fig. 2A). This would be consistent with our previous studies localizing TRPV1 to microglial cells in the rat retina.[53] Indeed clear examples of the typical amoeboid shape of microglia cell bodies were present in the outer retina and near the nerve fiber layer, where we reported them earlier.[53] Intense perinuclear staining also delineated the larger cell bodies of RGCs (Fig. 2A). This was confirmed by confocal microscopy of wholemount preparations counter-labeled with antibodies against heavy-chain neurofilaments that recognize large RGCs (Fig. 2B). This indicated punctate localization of TRPV1 to RGC dendrites, with more diffuse label in RGC cell bodies. Discrete TRPV1 localization was also apparent in small bundles of RGC axons in the peripheral retina, with denser distribution in large axon bundles near the optic nerve head (Figs. 2C, 2D). Smaller cell bodies also expressing TRPV1 near the nerve fiber layer were identified as microglia based on their amoeboid appearance.[53] This is shown explicitly in Figure 2E, where Iba-1 labeled microglia expressing TRPV1 are apparent on a background of TRPV1-labeled RGC axons. In RGC cultures, the pattern of TRPV1 localization was qualitatively similar to that observed in intact retina, with intense perinuclear and neurite staining (Fig. 2F). TRPV1 labeling appeared more robust on a per cell basis than that noted in intact retina, consistent with our PCR results (Fig. 1A). In the cell body, localization could correspond to plasma membrane and endoplasmic reticulum.[84–85] Similar to TRPV1 localization in situ, punctate clusters of intense label also highlighted RGC processes (Fig. 2F). Western blotting against TRPV1 with the same antibody confirmed its specificity in brain and whole retina from adult rat (Fig. 2G). Retina demonstrated a second, smaller band that differed in molecular weight by only a few kilodaltons, well within the 90- to 113-kDa range for various glycosylation states for this antibody.[79] Consistent with this, preabsorption of the TRPV1 antibody with a blocking peptide prevented the detection of all bands (Fig. 2G). Immunoblotting against actin served as a loading and a reaction control.

TRPV1 Activation and Pressure-Induced Death of RGCs

To test whether TRPV1 contributed directly to pressure-induced RGC apoptosis, we maintained RGCs under elevated hydrostatic pressure (+70 mm Hg) for 48 hours with increasing concentrations of the highly specific TRPV1 antagonist I-RTX,[53,66–70] and we measured changes in cell density and TUNEL reactivity (Fig. 3). We previously found that at this time point, +70 mm Hg produced the greatest decrease in RGC density and the greatest increase in fraction of TUNEL-positive cells.[18] Consistent with our published observations,[18] elevated pressure without I-RTX reduced the density of RGCs from ambient

levels by 36% ($P < 0.01$; Fig. 3A). Treatment with I-RTX significantly improved RGC density under pressure in a dose-dependent manner, with a 20% increase for 1 nM I-RTX ($P = 0.02$) and a 25% increase for 10 nM I-RTX ($P = 0.01$) compared with vehicle only (Fig. 3A). For these concentrations of I-RTX, ambient RGC density did not change compared with vehicle only ($P > 0.2$). With 10 nM I-RTX, density for RGCs under pressure reached ambient levels ($P = 0.98$). For the highest concentration of I-RTX (100 nM), RGC density under pressure actually decreased and was not statistically different from vehicle only ($P = 0.33$). However, this concentration of I-RTX also caused a 35% decrease for RGCs at ambient pressure compared with vehicle only ($P < 0.01$), so that the two pressure conditions were identical ($P = 0.12$).

Also consistent with our published observations,[18] elevated pressure without I-RTX induced to a twofold increase in the fraction of TUNEL-positive cells ($P < 0.01$; Fig. 3B). With increasing concentrations of I-RTX, the fraction of TUNEL-positive RGCs fluctuated slightly but did not change compared with vehicle only ($P \geq 0.06$; Fig. 3B). This suggests that the lower RGC density observed with the highest concentration of I-RTX (100 nM; Fig. 3A) might have resulted from a reduced ability to adhere to the culture plate, thereby artificially lowering the density measurements without inducing cell death. In support of this idea, for RGCs at elevated pressure, the fraction of TUNEL-positive cells steadily decreased with increasing concentrations of I-RTX by 20% to 51% compared with vehicle only ($P < 0.05$ for all; Fig. 3B). Thus, antagonism of TRPV1 with I-RTX reduced pressure-induced apoptosis of RGCs in a dose-dependent manner.

To test whether TRPV1 activation alone is capable of inducing RGC death, we applied increasing concentrations of the TRPV1-specific agonist capsaicin to RGCs for 48 hours and again assessed RGC density and TUNEL reactivity (Fig. 4). Treatment with capsaicin induced a gradual decrease in RGC density, with 1 μM capsaicin reducing RGC density by 27% ($P = 0.01$) and 100 μM reducing it by 58% ($P < 0.01$) compared with vehicle only. Correspondingly, capsaicin also induced a sharp increase in the fraction of TUNEL-positive RGCs, with 1 μM causing a twofold increase ($P < 0.01$) and 100 μM causing a 3.5-fold increase ($P < 0.01$) compared with vehicle. These data suggest that TRPV1 activation is capable of inducing RGC apoptosis in the absence of other insults.

Chelation of Extracellular Ca^{2+} and Pressure-Induced RGC Apoptosis

In other tissues, TRPV1 supports a strong Ca^{2+} conductance that leads to increased intracellular Ca^{2+}.[49–50,68,86–92] Increased intracellular Ca^{2+}, such as that associated with TRPV1 activation, can directly induce apoptotic cell death in many neuronal conditions.[93–100] If the effect of TRPV1 on the RGC response to pressure involves an influx of extracellular Ca^{2+}, a simple reduction in available Ca^{2+} should also protect RGCs. To test this, we reduced the concentration of extracellular Ca^{2+} available for influx using the Ca^{2+} chelator EGTA and measured changes in density and TUNEL-reactivity for RGCs at ambient or elevated pressure for 48 hours (Fig. 5). Based on our calculations, the 950-μM dose of EGTA reduced the concentration of available Ca^{2+} in the culture media from 1 mM to 100 μM. As before, elevated pressure induced a 35% decrease in RGC density ($P < 0.01$) that was accompanied by a twofold increase in the percentage of TUNEL-positive cells ($P < 0.01$; Figs. 5A, 5B). Although Ca^{2+} chelation at ambient pressure did not alter the density of RGCs ($P = 0.2$), it did decrease the baseline level of TUNEL-positive cells by 38% ($P < 0.01$; Fig. 5A). This suggests that the small degree of apoptosis that naturally occurred in our primary cultures was dependent on extracellular Ca^{2+} levels. For RGCs at elevated pressure, chelation of extracellular Ca^{2+} improved RGC survival with an 18% increase in density ($P < 0.05$) and a 56% decrease in TUNEL reactivity ($P < 0.01$) compared with no treatment (Fig. 5B). In fact, the fraction of TUNEL-positive cells reached the fraction at ambient pressure for the same concentration ($P = 0.04$; Fig. 5B). These data suggest that an influx of

extracellular Ca^{2+} is an important component of pressure-induced apoptosis in RGCs and that the contribution of TRPV1 to pressure-induced death may lie in its permeability to extracellular Ca^{2+}. We examine this possibility directly in the following experiment.

TRPV1 and Pressure-Induced Increases in RGC Ca^{2+}

Based on our results with EGTA, we examined whether exposure to elevated hydrostatic pressure could also increase RGC intracellular Ca^{2+} and whether TRPV1 activation could be involved. We exposed isolated RGCs to the Ca^{2+} indicator dye Fluo-4 at ambient or elevated pressure in the presence or absence of 100 nM I-RTX for 1 hour. This time was selected as the longest time for reliable detection and interpretation of Fluo-4 label.[53,83] Fluo-4 label in RGCs maintained at ambient pressure was modest, with a nearly uniform distribution of signal across a meshwork of neurites (Fig. 6A). This pattern resembled the node-like arrangement of TRPV1 in RGC axons and dendrites (Fig. 2). Exposure to elevated pressure dramatically increased Ca^{2+} in RGC cell bodies and processes, with puncta of localized changes particularly prominent in primary neurites (Fig. 6B). Specific antagonism of TRPV1 with 10 nM I-RTX greatly reversed most of the pressure-induced increases in accumulated Ca^{2+} (Fig. 6C). Treatment with I-RTX at ambient pressure also appeared to reduce the baseline intracellular Ca^{2+} in RGCs (Fig. 6D); this indicates that TRPV1 may play a role in maintaining normal levels of Ca^{2+} in RGCs. Quantification of total Fluo-4 revealed an almost fourfold increase in intensity with elevated pressure ($P < 0.01$) that was reduced by 40% after treatment with I-RTX ($P < 0.01$; Fig. 6E). I-RTX alone also decreased the baseline Ca^{2+} in RGCs by 71% ($P = 0.02$; Fig. 6E). These data suggest that increased intracellular Ca^{2+} because of TRPV1 activation is a prominent feature of the RGC response to elevated pressure.

TRPV1 in the DBA/2 Mouse Model of Glaucoma

To evaluate the potential relevance of TRPV1 to elevated IOP in an animal model of glaucoma, we examined TRPV1 localization in retina from age-matched DBA/2 mice (6 and 9 months) with different IOPs. DBA/2 mice have two ocular phenotypes that lead to elevated IOP: iris stromal atrophy and iris pigment dispersion caused by mutations in the *Tyrp1* and *Gpnmb* genes, respectively.[54,101,102] The retina from a 6-month-old DBA/2 with low IOP (average IOP, 14.85 mm Hg) displayed strong TRPV1 labeling in the large cell bodies of RGCs in the ganglion cell layer (Fig. 7A, top), much like in rat (Fig. 2). For a 9-month-old DBA/2 eye with slightly higher IOP (average IOP, 18.5 mm Hg), label was similarly intense in ganglion cells but with slightly increased signal in the nerve fiber layer (Fig. 7A, bottom). In addition, diffuse signal was apparent in the inner plexiform layer.

In a 6-month-old DBA/2 eye with higher IOP (average IOP, 17.7 mm Hg), the retina exhibited a notable increase in TRPV1 labeling in the inner plexiform layer, with less labeling near the ganglion cell bodies (Fig. 7B, top). Similarly, the retina from a 9-month-old DBA/2 eye with higher IOP (average IOP, 21.8 mm Hg) also had increased label in the inner plexiform layer compared with the lower IOP 9-month-old retina (Fig. 7B). This pattern could be attributed to a number of additional cell types or to a shift toward increased localization to RGC dendrites. In either case, these data suggest that changes in TRPV1 expression, particularly in the inner retina, can accompany increases in IOP in vivo. The difference in signal between the low and high IOP 6-month-old retinas was greater than that between the low and high IOP 9-month-old retina, not only because of the higher signal in the 9-month-old compared with the 6-month-old (Fig. 7A) low IOP retina but also less increase in label with elevated IOP at 9 months (Fig. 7B). In C57 mouse retina, TRPV1 localization to RGCs was similar to that in rat and DBA/2, with strong label in the ganglion cell and nerve fiber layers. There, TRPV1 colocalized with RGCs marked by immunolabel for Thy-1.1, a cell-surface marker in RGCs that localizes primarily to the cell body and axon

(Figs. 7C–E). Control experiments performed without the primary antibody resulted in an absence of label in all tissues (Fig. 7F). Western blotting against TRPV1, with actin as a control, confirmed the presence of TRPV1 in brain and retina from adult C57 mice (Fig. 7G). Unlike rat retina, mouse retina displays only one band at the expected molecular weight for TRPV1 (compare Fig. 7G with Fig. 2G). This suggests that the putative glycosylated form noted in samples of retina from adult rat is species specific rather than retina specific.

Discussion

Here we demonstrated that RGCs express the TRPV1 channel (Figs. 1, 2, 7) and that TRPV1 activation contributes to their death with exposure to hydrostatic pressure (Fig. 3). We also demonstrated that activation of TRPV1 alone was sufficient to induce apoptosis of RGCs (Fig. 4). Our experiments with EGTA showed that by chelating extracellular Ca^{2+}, we could dramatically reduce pressure-induced RGC apoptosis (Fig. 5). Through the same imaging paradigm that we used previously to demonstrate TRPV1-induced increases in microglia Ca^{2+},[53] we showed that elevated hydrostatic pressure increases RGC intracellular Ca^{2+} and that TRPV1 activation is an important component of this increase (Fig. 6). Finally, TRPV1 expression increases with IOP in the DBA/2 mouse model of glaucoma, and this appears to be independent of age (Fig. 7). Together our data suggest a novel role for TRPV1 as a contributor to the apoptotic response of RGCs to elevated hydrostatic pressure. Thus, TRPV1 could represent a novel target for therapeutic intervention in conditions involving elevated intraocular pressure.

Like other members of the TRP family, activation of TRPV1 leads to a potent influx of extracellular Ca^{2+} and subsequent membrane depolarization.[49–53,84–87] TRPV1-mediated Ca^{2+} influx leads to many intracellular events, including apoptotic cell death in epithelial cells of the lung[49,50] and in microglia of the brain.[52] TRPV1 activation is also linked to the release of Ca^{2+} from intracellular stores.[103] Interestingly, chelation of extracellular Ca^{2+} nearly reversed completely pressure-induced apoptosis of RGCs (Fig. 5), whereas pharmacologic interference of TRPV1 function afforded only partial protection (Fig. 3). These findings suggest that other Ca^{2+}-permeable channels are involved in the RGC apoptotic response to pressure, some of which may be influenced by the activation of TRPV1. In dorsal root ganglion neurons, the activation of TRPV1 inhibits conductance through most voltage-dependent Ca^{2+} channels and causes rapid internalization of voltage-gated Ca^{2+} channels through Ca^{2+}-dependent activation of the protein phosphatase calcineurin.[104–106] In glaucoma, the cleavage of calcineurin occurs in response to elevated IOP, and inhibiting calcineurin systemically inhibits pressure-induced RGC axon loss in the optic nerve.[107] We previously found that Bcl-2, which increases the Ca^{2+}-buffering capacity of mitochondria,[108] increases threefold in RGCs exposed to elevated hydrostatic pressure.[18] For years it has been recognized that many drugs used to lower IOP or reduce vasoconstriction in glaucoma also affect RGCs by modulating the accumulation of intracellular Ca^{2+}.[109] Similarly, studies of pressure-related ischemic injury at the optic nerve head indicate that the influx of extracellular Ca^{2+} into the RGC axoplasm is critical to the development of abnormality from the ischemic insult.[110,111]

Various TRP subunits are activated by mechanical stimuli in many tissues, including osmotic stress in the kidney, mechanical force in the heart and vasculature, pressure in the inner ear, and mechanical force in afferent fibers of the colon.[28,36,42,112,113] TRPV1 subunits in multiple sensory ganglia of the spinal cord respond to the transduction of mechanical stimuli involved in several systemic functions, including monitoring of pressure-induced pain and injury.[46] Importantly, TRPV1 is implicated in sensing changes in intraluminal hydrostatic pressure in vascular walls and in mediating the response of jejunal afferents to pressure-induced distension of the gut.[40,41] TRPV1 is also necessary for

mediating mechanosensitivity in colon afferents.[43] We have shown that TRPV1 expressed by retinal microglia contributes to pressure-induced nuclear translocation of NFκB and increased secretion of the inflammatory cytokine IL-6.[53] Thus, our hypothesis that TRPV1 contributes to the apoptotic response of RGCs to pressure is not without precedence.

In the goldfish and zebrafish retina, TRPV1 expression seems to be restricted to photoreceptors,[114] whereas our analysis of rat and mouse retina revealed robust TRPV1 localization in the ganglion cell and nerve fiber layers (Figs. 2, 7). Our findings very closely resemble the localization of TRPV-L1 (TRPV2) in rat, cat, and primate retina.[115] In some regions of the cat and primate retina, TRPV-L1 expression is restricted to the ganglion cell layer.[115] We do not rule out the localization of TRPV1 in the outer retina of the rodent; indeed, some of our unpublished findings suggest weak expression there (data not shown). Our analysis of the DBA/2 retina revealed that increased IOP led to a dramatic increase in TRPV1 localization, especially in the inner retina, at 6 and 9 months of age (Fig. 7). Although Müller cell expression could account for a portion of TRPV1 immunoreactivity in the inner plexiform layer, it is possible that the increase in signal in this region is attributed to a change in dendritic expression of TRPV1 in RGCs. This change could reflect a recombination of TRPV1 with other TRP subunits or could represent a compensatory response caused by progressive changes in intracellular Ca^{2+} homeostasis. The increase in TRPV1 label with IOP was less dramatic at 9 months than at 6 months (Fig. 7B). If indeed the shift to the inner plexiform layer is indicative of RGC dendritic labeling, this difference between the 6- and 9-month higher IOP retinas could be explained by dendritic pruning with age. However, a larger sample is necessary to draw hard conclusions. Interestingly, the downregulation of TRPV1 expression in whole retina was noted after IOP-induced ischemic-reperfusion injury in rats.[116] Based on our histologic assessment of TRPV1 expression, it appears that IOP-dependent changes in TRPV1 are layer specific, which may not be apparent in whole retina protein and mRNA analysis. TRPV1 is known to localize to the endoplasmic reticulum and the plasma membrane[84,85]; therefore, it is possible that dendritic expression constitutes a shift in localization without a significant change in expression level.

Given the important contribution of TRPV1 to a variety of Ca^{2+}- and pressure-dependent processes, it is logical to propose a role for it in the RGC response to hydrostatic pressure. In a fluid-based environment such as the retina, pressure is translated to aqueous shear at the cell membrane, in accordance with LaPlace's Law.[117] In glaucoma, a popular hypothesis is that elevated pressure in the eye is translated to mechanical stress at the optic nerve head, which, in turn, can affect reperfusion pressure in the retina.[9] Our results indicate TRPV1 localization throughout the RGC, including the axon (Fig. 2), and any compartment could potentially contribute to the pressure response. Yet, we do not understand how pressure translates to neuronal apoptosis. All cells, including neurons, undergo extensive intracellular activity in response to most mechanical stimuli, including pressure.[118] A large body of literature in biomechanics indicates that the overwhelming contributor to compression-related cellular stress is increased hydrostatic pressure. This is so in cardiac vessels, lung, kidney, and gut.[117,119,120] For our RGCs, which are plated on a rigid surface, applied pressure represents a uniform hydrostatic load (i.e., air pressure distributed equally above a small-volume liquid column), and this is known to induce membrane compression.[117] For such a configuration, careful mathematical analysis indicates that the pressure gradient between the plates and the liquid column is substantial, even for less elastic tissue such as cartilage.[117,119,120] In this case, the most likely sources of cellular perturbation are distortional tension, hydrostatic compression, and the gradient of liquid potential across the cell membrane.[117] These perturbations are known to disrupt the actin cytoskeletal scaffolding, which can increase the conductance of channels sensitive to mechanical tension.[121] Thus, though we propose that TRPV1 in RGCs can be activated by pressure and

contributes to a pressure-dependent signal, we do not know whether this activation arises from static pressure regardless of magnitude, changes in pressure or a pressure gradient, hydrostatic shear at the cell membrane, or an aqueous gradient arising from increased pressure. Another possibility is that TRPV1 is activated not primarily by pressure but secondarily by intracellular activation through another receptor.

Although direct, mechanical activation of TRPV1 is an intriguing possibility, activation of TRPV1 could also occur indirectly at any point within the pressure-induced degenerative pathway. For example, TRPV1 in vivo could also be activated by ligands endogenous to the retina, such as endothelin-1, which is a potent vasoconstrictor that potentiates TRPV1 activity.[122] The endothelin receptor is also upregulated in the glaucomatous eye,[123] and endothelin can directly induce glaucomatous loss of RGCs.[124] The endocannabinoid anandamide is also known to activate TRPV1 in a rat model of IOP-induced ischemic-reperfusion injury. In this model, intravitreal injection of the TRPV1 antagonist capsazepine reversed the protective effects of a stable anandamide analogue on RGC death.[116] This could have bearing on the results of our imaging experiments, which suggest that TRPV1 contributes to baseline Ca^{2+} levels at ambient pressure (Fig. 6D). Even so, it is important to note that while the examination of anandamide and TRPV1 was conducted in vivo, our work assesses RGC-specific and retina-specific responses to TRPV1 inhibition without the extraretinal milieu of the globe. Although there is no doubt that RGCs are capable of responding to anandamide and intravitreal injection of the capsazepine, our data suggest that other cell types, including cells of the vasculature, could also respond (data not shown). In this case, vasculature-specific responses could contribute to the effects of capsazepine on RGC death. This is particularly intriguing given that the capsazepine study was conducted in the context of an ischemic-reperfusion injury.

Acknowledgments

The authors thank Brian J. Carlson and Julie Y. Koh (Vanderbilt University Medical Center, Nashville, TN) for technical support in the execution of these studies. Micrographs were obtained with the aid of the Cell Imaging Core at Vanderbilt University Medical Center.

Supported by the Melza M. and Frank Theodore Barr Foundation through the Glaucoma Research Foundation Catalyst for a Cure initiative (DJC); National Institutes of Health Grant EY017427 (DJC); a Challenge Grant and a Wasserman Award from Research to Prevent Blindness, Inc. (DJC); Vanderbilt Vision Research Center National Eye Institute Core Grant 5P30EY008126–19; and a fellowship from Fight for Sight, Inc. (RMS).

References

1. Kung C. A possible unifying principle for mechanosensation. Nature. 2005; 436:647–654. [PubMed: 16079835]
2. Kalapesi FB, Tan JC, Coroneo MT. Stretch-activated channels: a mini-review. Are stretch-activated channels an ocular barometer? Clin Exp Ophthalmol. 2005; 33:210–217.
3. Ostrow LW, Sachs F. Mechanosensation and endothelin in astrocytes— hypothetical roles in CNS pathophysiology. Brain Res Brain Res Rev. 2005; 48:488–508. [PubMed: 15914254]
4. Lumpkin EA, Bautista DM. Feeling the pressure in mammalian somatosensation. Curr Opin Neurobiol. 2005; 15:382–388. [PubMed: 16023849]
5. Heppenstall PA, Lewin GR. A role for T-type Ca^{2+} channels in mechanosensation. Cell Calcium. 2006; 40:165–174. [PubMed: 16777219]
6. Wemmie JA, Price MP, Welsh MJ. Acid-sensing ion channels: advances, questions and therapeutic opportunities. Trends Neurosci. 2006; 29:578–586. [PubMed: 16891000]
7. Lansman JB, Franco-Obregon A. Mechanosensitive ion channels in skeletal muscle: a link in the membrane pathology of muscular dystrophy. Clin Exp Pharmacol Physiol. 2006; 33:649–656. [PubMed: 16789935]

8. Jay JL, Murdoch JR. The rate of visual field loss in untreated primary open angle glaucoma. Br J Ophthalmol. 1993; 77:176–178. [PubMed: 8457511]
9. Quigley HA. Neuronal death in glaucoma. Prog Retin Eye Res. 1999; 18:39–57. [PubMed: 9920498]
10. Jonas JB, Budde WM. Diagnosis and pathogenesis of glaucomatous optic neuropathy: morphological aspects. Prog Retinal Eye Res. 2000; 19:1–40.
11. Quigley HA, Broman AT. The number of people with glaucoma worldwide in 2010 and 2020. Br J Ophthalmol. 2006; 90:262–267. [PubMed: 16488940]
12. Emi K, Pederson JE, Toris CB. Hydrostatic pressure of the suprachoroidal space. Invest Ophthalmol Vis Sci. 1989; 30:233–238. [PubMed: 2914753]
13. Morgan WH, Yu DY, Cooper RL, Alder VA, Cringle SJ, Constable IJ. The influence of cerebrospinal fluid pressure on the lamina cribrosa tissue pressure gradient. Invest Ophthalmol Vis Sci. 1995; 36:1163–1172. [PubMed: 7730025]
14. Tezel G, Wax MB. Increased production of tumor necrosis factor-α by glial cells exposed to simulated ischemia or elevated hydrostatic pressure induces apoptosis in cocultured retinal ganglion cells. J Neurosci. 2000; 20:8693–8700. [PubMed: 11102475]
15. Wax MB, Tezel G, Kobayashi S, Hernandez MR. Responses of different cell lines from ocular tissues to elevated hydrostatic pressure. Br J Ophthalmol. 2000; 84:423–428. [PubMed: 10729303]
16. Liu Q, Ju WK, Crowston JG, et al. Oxidative stress is an early event in hydrostatic pressure induced retinal ganglion cell damage. Invest Ophthalmol Vis Sci. 2007; 48:4580–4589. [PubMed: 17898281]
17. Agar A, Li S, Agarwal N, Coroneo MT, Hill MA. Retinal ganglion cell line apoptosis induced by hydrostatic pressure. Brain Res. 2006; 1086:191–200. [PubMed: 16638612]
18. Sappington RM, Chan M, Calkins DJ. Interleukin-6 protects retinal ganglion cells from pressure-induced death. Invest Ophthalmol Vis Sci. 2006; 47:2932–2942. [PubMed: 16799036]
19. Garcia-Valenzuela E, Shareef S, Walsh J, Sharman SC. Programmed cell death of retinal ganglion cells during experimental glaucoma. Exp Eye Res. 1995; 61:33–44. [PubMed: 7556468]
20. Quigley HA, Nickells RW, Kerrigan LA, Pease ME, Thibault DJ, Zack DJ. Retinal ganglion cell death in experimental glaucoma and after axotomy occurs by apoptosis. Invest Ophthalmol Vis Sci. 1995; 36:774–786. [PubMed: 7706025]
21. Farkas RH, Grosskreutz CL. Apoptosis, neuroprotection and retinal ganglion cell death: an overview. Int Ophthalmol Clin. 2001; 41:111–130. [PubMed: 11198138]
22. Wang X, Tay SS, Ng YK. c-fos and c-jun expression in nitric oxide synthase immunoreactive neurons in the lateral geniculate nucleus of experimental glaucomatous rats. Exp Brain Res. 2002; 144:365–372. [PubMed: 12021818]
23. Hanninen VA, Pantcheva MB, Freeman EE, Poulin NR, Grosskreutz CL. Activation of caspase 9 in a rat model of experimental glaucoma. Curr Eye Res. 2002; 25:389–395. [PubMed: 12789547]
24. Guo L, Moss SE, Alexander RA, Ali RR, Fitzke FW, Cordeiro MF. Retinal ganglion cell apoptosis in glaucoma is related to intraocular pressure and IOP-induced effects on extracellular matrix. Invest Ophthalmol Vis Sci. 2005; 46:175–182. [PubMed: 15623771]
25. Levkovitch-Verbin H, Quigley HA, Martin KR, et al. The transcription factor c-jun is activated in retinal ganglion cells in experimental rat glaucoma. Exp Eye Res. 2005; 80:663–670. [PubMed: 15862173]
26. Minke B, Cooke B. TRP channel proteins and signal transduction. Physiol Rev. 2002; 82:429–472. [PubMed: 11917094]
27. Corey DP. New TRP channels in hearing and mechanosensation. Neuron. 2003; 39:585–588. [PubMed: 12925273]
28. Corey DP, Garcia-Anoveros J, Holt JR, et al. TRPA1 is a candidate for the mechanosensitive transduction channel of vertebrate hair cells. Nature. 2004; 432:723–730. [PubMed: 15483558]
29. Moran MM, Xu H, Clapham DE. TRP ion channels in the nervous system. Curr Opin Neurobiol. 2004; 14:362–369. [PubMed: 15194117]
30. Pan HL, Chen SR. Sensing tissue ischemia: another new function for capsaicin receptors? Circulation. 2004; 110:1826–1831. [PubMed: 15364816]

31. Wang GX, Poo MM. Requirement of TRPC channels in netrin-1-induced chemotropic turning of nerve growth cones. Nature. 2005; 434:898–904. [PubMed: 15758951]
32. Lin S-Y, Corey DP. TRP channels in mechanosensation. Curr Opin Neurobiol. 2005; 15:350–357. [PubMed: 15922584]
33. O'Neil RG, Heller S. The mechanosensitive nature of TRPV channels. Pflugers Arch Eur J Physiol. 2005; 451:193–203. [PubMed: 15909178]
34. Liedtke W. TRPV4 plays an evolutionary conserved role in the transduction of osmotic and mechanical stimuli in live animals. J Physiol. 2005; 567:53–58. [PubMed: 15961428]
35. Pingle SC, Matta JA, Ahern GP. Capsaicin receptor: TRPV1 a promiscuous TRP channel. Handb Exp Pharmacol. 2007; 179:155–171. [PubMed: 17217056]
36. Birder LA, Nakamura Y, Kiss S, et al. Altered urinary bladder function in mice lacking the vanilloid receptor TRPV1. Nat Neurosci. 2002; 5:856–860. [PubMed: 12161756]
37. Mutai H, Heller S. Vertebrate and invertebrate TRPV-like mechanoreceptors. Cell Calcium. 2003; 33:471–478. [PubMed: 12765692]
38. Helyes Z, Szabo A, Nemeth J, et al. Antiinflammatory and analgesic effects of somatostatin released from capsaicin-sensitive sensory nerve terminals in a Freund's adjuvant-induced chronic arthritis model in the rat. Arthritis Rheum. 2004; 50:1677–1685. [PubMed: 15146439]
39. Hwang SJ, Burette A, Rustioni A, Valtschanoff JG. Vanilloid receptor VR1-positive primary afferents are glutamatergic and contact spinal neurons that co-express neurokinin receptor NK1 and glutamate receptors. J Neurocytol. 2004; 33:321–329. [PubMed: 15475687]
40. Rong W, Hillsley K, Davis JB, Hicks G, Winchester WJ, Grundy D. Jejunal afferent nerve sensitivity in wild-type and TRPV1 knockout mice. J Physiol. 2004; 560:867–881. [PubMed: 15331673]
41. Scotland RW, Sanderson MJ. Vanilloid receptor TRPV1, sensory C-fibers, and vascular autoregulation: a novel mechanism involved in myogenic constriction. Circ Res. 2004; 95:1027–1034. [PubMed: 15499026]
42. Brierley SM, Carter R, Jones W 3rd, et al. Differential chemosensory function and receptor expression of splanchnic and pelvic colonic afferents in mice. J Physiol. 2005; 567:267–281. [PubMed: 15946967]
43. Jones RC 3rd, Xu L, Gebhart GF. The mechanosensitivity of mouse colon afferent fibers and their sensitization by inflammatory mediators require transient receptor potential vanilloid 1 and acid-sensing ion channel 3. J Neurosci. 2005; 25:10981–10989. [PubMed: 16306411]
44. Ma W, Zhang Y, Bantel C, Eisenach JC. Medium and large injured dorsal root ganglion cells increase TRPV-1, accompanied by increased α2C-adrenoceptor co-expression and functional inhibition by clonidine. Pain. 2005; 113:386–394. [PubMed: 15661448]
45. Szabo A, Helyes Z, Sandor K, et al. Role of transient receptor potential vanilloid 1 receptors in adjuvant-induced chronic arthritis: in vivo study using gene-deficient mice. J Pharmacol Exp Ther. 2005; 314:111–119. [PubMed: 15831443]
46. Plant TD, Zollner C, Mousa SA, Oksche A. Endothelin-1 potentiates capsaicin-induced TRPV1 currents via the endothelin A receptor. Exp Biol Med. 2006; 231:1161–1164.
47. Liedtke W. Transient receptor potential vanilloid channels functioning in transduction of osmotic stimuli. J Endocrinol. 2006; 191:515–523. [PubMed: 17170210]
48. Daly D, Rong W, Chess-Williams R, Chapple C, Grundy D. Bladder afferent sensitivity in wild-type and TRPV1 knockout mice. J Physiol. 2007; 583:663–674. [PubMed: 17627983]
49. Agopyan N, Head J, Yu S, Simon SA. TRPV1 receptors mediate particulate matter-induced apoptosis. Am J Physiol Lung Cell Mol Physiol. 2004; 286:L563–L572. [PubMed: 14633515]
50. Reilly CA, Johansen ME, Lanza DL, Lee J, Lim JO, Yost GS. Calcium-dependent and independent mechanisms of capsaicin receptor (TRPV1)-mediated cytokine production and cell death in human bronchial epithelial cells. J Biochem Mol Toxicol. 2005; 19:266–275. [PubMed: 16173059]
51. Aarts MM, Tymianski M. TRPMs and neuronal cell death. Pflugers Arch Eur J Physiol. 2005; 451:243–249. [PubMed: 16044308]
52. Kim SR, Kim SU, Oh U, Jin BK. Transient receptor potential vanilloid subtype 1 mediates microglial cell death in vivo and in vitro via Ca^{2+}-mediated mitochondrial damage and cytochrome *c* release. J Immunol. 2006; 177:4322–4329. [PubMed: 16982866]

53. Sappington RM, Calkins D. TRPV1 contributes to microglia-derived IL-6 and NFκb translocation with elevated hydrostatic pressure. Invest Ophthalmol Vis Sci. 2008; 49:3004–3017. [PubMed: 18362111]
54. Inman DM, Sappington RM, Horner PJ, Calkins DJ. Quantitative correlation of optic nerve pathology with ocular pressure and corneal thickness in the DBA/2 mouse model of glaucoma. Invest Ophthalmol Vis Sci. 2006; 47:986–996. [PubMed: 16505033]
55. Mukai S, Mishima HK, Shoge K, Shinya M, Ishihara K, Sasa M. Existence of ionotropic glutamate receptor subtypes in cultured rat retinal ganglion cells obtained by the magnetic cell sorter method and inhibitory effects of 20-hydroxyecdysone, a neurosteroid, on the glutamate response. Jpn J Pharmacol. 2002; 89:44–52. [PubMed: 12083742]
56. Farkas RH, Qian J, Goldberg JL, Quigley HA, Zack DJ. Gene expression profiling of purified rat retinal ganglion cells. Invest Ophthalmol Vis Sci. 2004; 45:2503–2513. [PubMed: 15277470]
57. Goldberg JL, Espinosa JS, Xu Y, Davidson N, Kovacs GT, Barres BA. Retinal ganglion cells do not extend axons by default: promotion by neurotrophic signaling and electrical activity. Neuron. 2002; 33:689–702. [PubMed: 11879647]
58. Goldberg JL, Vargas ME, Wang JT, et al. An oligodendrocyte lineage-specific semaphorin, Sema5A, inhibits axon growth by retinal ganglion cells. J Neurosci. 2004; 24:4989–4999. [PubMed: 15163691]
59. Kerrison JB, Zack DJ. Neurite outgrowth in retinal ganglion cell culture. Methods Mol Biol. 2007; 356:427–434. [PubMed: 16988421]
60. Kerrison JB, Lewis RN, Otteson DC, Zack DJ. Bone morphogenetic proteins promote neurite outgrowth in retinal ganglion cells. Mol Vis. 2005; 11:208–215. [PubMed: 15788999]
61. Yu ZK, Chen YN, Aihara M, Mao W, Uchida S, Araie M. Effects of beta-adrenergic receptor antagonists on oxidative stress in purified rat retinal ganglion cells. Mol Vis. 2007; 13:833–839. [PubMed: 17615544]
62. Perry VH, Henderson Z, Linden R. Postnatal changes in retinal ganglion cell and optic axon populations in the pigmented rat. J Comp Neurol. 1983; 219:356–368. [PubMed: 6619343]
63. Dreher B, Potts RA, Bennett MR. Evidence that the early postnatal reduction in the number of rat retinal ganglion cells is due to a wave of ganglion cell death. Neurosci Lett. 1983; 36:255–260. [PubMed: 6866331]
64. Hernández M, Guerrikagoitia I, Martínez-Millan L, Vecino E. NMDA-receptor blockade enhances cell apoptosis in the developing retina of the postnatal rat. Int J Dev Biol. 2007; 51:117–122. [PubMed: 17294362]
65. Sappington RM, Calkins DJ. Elevated pressure induces proteosome-dependent secretion of IL-6 and activation of NFκB in retinal glial cells. Invest Ophthalmol Vis Sci. 2006; 47:3860–3869. [PubMed: 16936098]
66. Wahl P, Foged C, Tullin S, Thomsen C. Iodo-resiniferatoxin, a new potent vanilloid receptor antagonist. Mol Pharmacol. 2001; 59:9–15. [PubMed: 11125018]
67. Starowicz K, Maione S, Cristino L, et al. Tonic endovanilloid facilitation of glutamate release in brainstem descending antinociceptive pathways. J Neurosci. 2007; 27:13739–13749. [PubMed: 18077685]
68. Rigoni M, Trevisani M, Gazzieri D, et al. Neurogenic responses mediated by vanilloid receptor-1 (TRPV1) are blocked by the high affinity antagonist, iodo-resiniferatoxin. Br J Pharmacol. 2003; 138:977–985. [PubMed: 12642400]
69. Undem BJ, Kollarik M. Characterization of the vanilloid receptor 1 antagonist iodo-resiniferatoxin on the afferent and efferent function of vagal sensory C-fibers. J Pharmacol Exp Ther. 2002; 303:716–722. [PubMed: 12388656]
70. Seabrook GR, Sutton KG, Jarolimek W, et al. Functional properties of the high-affinity TRPV1 (VR1) vanilloid receptor antagonist (4-hydroxy-5-iodo-3-methoxyphenylacetate ester) iodo-resiniferatoxin. J Pharmacol Exp Ther. 2002; 303:1052–1060. [PubMed: 12438527]
71. Otten U, Lorez HP, Businger F. Nerve growth factor antagonizes the neurotoxic action of capsaicin on primary sensory neurones. Nature. 1983; 301:515–517. [PubMed: 6185853]

72. Holzer P. Local effector functions of capsaicin-sensitive sensory nerve endings: involvement of tachykinins, calcitonin gene-related peptide and other neuropeptides. Neuroscience. 1988; 24:739–768. [PubMed: 3288903]
73. Bevan S, Szolcsányi J. Sensory neuron-specific actions of capsaicin: mechanisms and applications. Trends Pharmacol Sci. 1990; 11:330–333. [PubMed: 2203194]
74. Bers DM. A simple method for the accurate determination of free [Ca] in Ca-EGTA solutions. Am J Physiol. 1982; 242:C404–C408. [PubMed: 6805332]
75. Harvey DM, Calkins DJ. Localization of kainate receptors to the presynaptic active zone of the rod photoreceptor in primate retina. Vis Neurosci. 2002; 19:681–692. [PubMed: 12507334]
76. Liapi A, Wood JN. Extensive co-localization and heteromultimer formation of the vanilloid receptor-like protein TRPV2 and the capsaicin receptor TRPV1 in the adult rat cerebral cortex. Eur J Neurosci. 2005; 22:825–834. [PubMed: 16115206]
77. Aoki Y, Ohtori S, Takahashi K, et al. Expression and co-expression of VR1, CGRP, and IB4-binding glycoprotein in dorsal root ganglion neurons in rats: differences between the disc afferents and the cutaneous afferents. Spine. 2005; 30:1496–1500. [PubMed: 15990662]
78. Stein AT, Ufret-Vincenty CA, Hua L, Santana LF, Gordon SE. Phosphoinositide 3-kinase binds to TRPV1 and mediates NGF-stimulated TRPV1 trafficking to the plasma membrane. J Gen Physiol. 2006; 128:509–522. [PubMed: 17074976]
79. Wang C, Hu HZ, Colton CK, Wood JD, Zhu MX. An alternative splicing product of the murine *trpv1* gene dominant negatively modulates the activity of TRPV1 channels. J Biol Chem. 2004; 279:37423–37430. [PubMed: 15234965]
80. Woodbury CJ, Zwick M, Wang S, et al. Nociceptors lacking TRPV1 and TRPV2 have normal heat responses. J Neurosci. 2004; 24:6410–6415. [PubMed: 15254097]
81. Sharif Naeini R, Witty MF, Séguéla P, Bourque CW. An N-terminal variant of Trpv1 channel is required for osmosensory transduction. Nat Neurosci. 2006; 9:93–98. [PubMed: 16327782]
82. Calkins DJ, Sappington RM, Hendry SH. Morphological identification of ganglion cells expressing the alpha subunit of type II calmodulin-dependent protein kinase in the macaque retina. J Comp Neurol. 2005; 481:194–209. [PubMed: 15562509]
83. Gee KR, Brown KA, Chen WN, Bishop-Stewart J, Gray D, Johnson I. Chemical and physiological characterization of fluo-4 Ca(2+)-indicator dyes. Cell Calcium. 2000; 27:97–106. [PubMed: 10756976]
84. Liu M, Liu MC, Magoulas C, Priestley JAV, Willmott NJ. Versatile regulation of cytosolic Ca^{2+} by vanilloid receptor-1 in rat dorsal root ganglion neurons. J Biol Chem. 2003; 278:5462–5472. [PubMed: 12454015]
85. Marshall ICB, Owen DE, Cripps TV, Davis JB, McNulty S, Smart D. Activation of vanilloid receptor 1 by resiniferatoxin mobilizes calcium from inositol 1,4,5-triphosphate-sensitive stores. Br J Pharmacol. 2003; 138:172–176. [PubMed: 12522087]
86. Yoon J, Ben-Ami HC, Hong YS, et al. Novel mechanism of massive photoreceptor degeneration caused by mutations in the *trp* gene of *Drosophila*. J Neurosci. 2000; 20:649–659. [PubMed: 10632594]
87. Hong YS, Park S, Geng C, et al. Single amino acid change in the fifth transmembrane segment of the TRP Ca^{2+} channel causes massive degeneration of photoreceptors. J Biol Chem. 2002; 277:33884–33889. [PubMed: 12107168]
88. Puntambekar P, Van Buren J, Raisinghani M, Premkumar LS, Ramkumar V. Direct interaction of adenosine with the TRPV1 channel protein. J Neurosci. 2004; 24:3663–3671. [PubMed: 15071115]
89. Lakshmi S, Joshi PG. Co-activation of P2Y2 receptor and TRPV channel by ATP: implications for ATP induced pain. Cell Mol Neurobiol. 2005; 25:819–832. [PubMed: 16133936]
90. van der Stelt M, Trevisani M, Vellani V, et al. Anandamide acts as an intracellular messenger amplifying Ca2+ influx via TRPV1 channels. EMBO J. 2005; 24:3026–3037. [PubMed: 16107881]
91. El Kouhen R, Surowy CS, Bianchi BR, et al. A-425619 [1-isoquinolin-5-yl-3-(4-trifluoromethyl-benzyl)-urea], a novel and selective transient receptor potential type V1 receptor antagonist, blocks

channel activation by vanilloids, heat, and acid. J Pharmacol Exp Ther. 2005; 314:400–409. [PubMed: 15837819]

92. Toth A, Wang Y, Kedei N, et al. Different vanilloid agonists cause different patterns of calcium response in CHO cells heterologously expressing rat TRPV1. Life Sci. 2005; 76:2921–2932. [PubMed: 15820503]
93. Stout AK, Raphael HM, Kanterewicz BI, Klann E, Reynolds IJ. Glutamate-induced neuron death requires mitochondrial calcium uptake. Nat Neurosci. 1998; 1:366–373. [PubMed: 10196525]
94. Kass GEN, Orrenius S. Calcium signaling and cytotoxicity. Environ Health Perspect. 1999; 107:25–35. [PubMed: 10229704]
95. Hajnoczky G, Davies E, Madesh M. Calcium signaling and apoptosis. Biochem Biophys Res Commun. 2003; 304:445–454. [PubMed: 12729578]
96. Verkhratsky A, Toescu EC. Endoplasmic reticulum Ca^{2+} homeostasis and neuronal death. J Cell Mol Med. 2003; 7:351–361. [PubMed: 14754504]
97. Arundine M, Tymianski M. Molecular mechanisms of calcium-dependent neurodegeneration in excitotoxicity. Cell Calcium. 2003; 34:325–337. [PubMed: 12909079]
98. Weber JT. Calcium homeostasis following traumatic neuronal injury. Curr Neurovasc Res. 2004; 1:151–171. [PubMed: 16185191]
99. Coleman M. Axon degeneration mechanisms: commonality amid diversity. Nat Rev Neurosci. 2005; 6:889–898. [PubMed: 16224497]
100. Chinopoulos C, Adam-Vizi V. Calcium, mitochondria and oxidative stress in neuronal pathology: novel aspects of an enduring theme. FEBS Lett. 2006; 273:433–450.
101. Chang B, Smith RS, Hawes NL, et al. Interacting loci cause severe iris atrophy and glaucoma in DBA/2J mice. Nat Genet. 1999; 21:405–409. [PubMed: 10192392]
102. John SW, Smith RS, Savinova OV, et al. Essential iris atrophy, pigment dispersion, and glaucoma in DBA/2J mice. Invest Ophthalmol Vis Sci. 1998; 39:951–962. [PubMed: 9579474]
103. Eun SY, Jung SJ, Park YK, Kwak J, Kim SJ, Kim J. Effects of capsaicin on Ca(2+) release from the intracellular Ca(2+) stores in the dorsal root ganglion cells of adult rats. Biochem Biophys Res Commun. 2001; 285:1114–1120. [PubMed: 11478769]
104. Hagenacker T, Splettstoesser F, Greffrath W, Treede RD, Busselberg D. Capsaicin differentially modulates voltage-activated calcium currents in dorsal root ganglion neurons of rats. Brain Res. 2005; 1062:74–85. [PubMed: 16269136]
105. Wu ZZ, Chen SR, Pan HL. Transient receptor potential vanilloid type 1 activation down-regulates voltage-gated calcium channels through calcium-dependent calcineurin in sensory neurons. J Biol Chem. 2005; 280:18142–18151. [PubMed: 15746091]
106. Wu ZZ, Chen SR, Pan HL. Signaling mechanisms of down-regulation of voltage-activated Ca^{2+} channels by transient receptor potential vanilloid type 1 stimulation with olvanil in primary sensory neurons. Neuroscience. 2006; 141:407–419. [PubMed: 16678970]
107. Huang W, Fileta JB, Dobberfuhl A, et al. Calcineurin cleavage is triggered by elevated intraocular pressure, and calcineurin inhibition blocks retinal ganglion cell death in experimental glaucoma. Proc Natl Acad Sci U S A. 2005; 102:12242–12247. [PubMed: 16103353]
108. Rodnitzky RL. Can calcium antagonists provide a neuroprotective effect in Parkinson's disease? Drugs. 1999; 57:845–849. [PubMed: 10400399]
109. Ishii K, Matsuo H, Fukaya Y, et al. Iganidipine, a new watersoluble Ca^{2+} antagonist: ocular and periocular penetration after instillation. Invest Ophthalmol Vis Sci. 2003; 44:1169–1177. [PubMed: 12601046]
110. Stys PK, Waxman SG, Ransom BR. Ionic mechanisms of anoxic injury in mammalian CNS white matter: role of Na+ channels and Na(+)-Ca2+ exchanger. J Neurosci. 1992; 12:430–439. [PubMed: 1311030]
111. Whitmore AV, Libby RT, John SW. Glaucoma: thinking in new ways—a role for autonomous axonal self-destruction and other compartmentalised processes? Prog Retin Eye Res. 2005; 24:639–662. [PubMed: 15953750]
112. Liedtke W, Choe Y, Marti-Renom MA, et al. Vanilloid receptor-related osmotically activated channel (VR-OAC), a candidate vertebrate osmoreceptor. Cell. 2000; 103:525–535. [PubMed: 11081638]

113. Nauli SM, Alenghat FJ, Luo Y, et al. Polycystins 1 and 2 mediate mechanosensation in the primary cilium of kidney cells. Nat Genet. 2003; 33:129–137. [PubMed: 12514735]
114. Zimov S, Yazulla S. Localization of vanilloid receptor 1 (TRPV1/VR1)-like immunoreactivity in goldfish and zebrafish retinas: restriction to photoreceptor synaptic ribbons. J Neurocytol. 2004; 33:441–452. [PubMed: 15520529]
115. Yazulla S, Studholme KM. Vanilloid receptor like 1 (VRL1) immunoreactivity in mammalian retina: colocalization with somatostatin and purinergic P2X1 receptors. J Comp Neurol. 2004; 474:407–418. [PubMed: 15174083]
116. Nucci C, Gasperi V, Tartaglione R, et al. Involvement of the endocannabinoid system in retinal damage after high intraocular pressure-induced ischemia in rats. Invest Ophthalmol Vis Sci. 2007; 48:2997–3004. [PubMed: 17591864]
117. Tanck E, van Driel WD, Hagen JW, Burger EH, Blankevoort L, Huiskes R. Why does intermittent hydrostatic pressure enhance the mineralization process in fetal cartilage? J Biomech. 1999; 32:153–161. [PubMed: 10052920]
118. Trepat X, Deng L, An SS, et al. Universal physical responses to stretch in the living cell. Nature. 2007; 447:592–595. [PubMed: 17538621]
119. Kaarniranta K, Elo M, Sironen R, et al. Hsp70 accumulation in chondrocytic cells exposed to high continuous hydrostatic pressure coincides with mRNA stabilization rather than transcriptional activation. Proc Natl Acad Sci U S A. 1998; 95:2319–2324. [PubMed: 9482883]
120. Brown TD. Techniques for mechanical stimulation of cells in vitro: a review. J Biomech. 2000; 33:3–14. [PubMed: 10609513]
121. Wan X, Juranka P, Morris CE. Activation of mechanosensitive currents in traumatized membrane. Am J Physiol. 1999; 276(pt 1):C318–C327. [PubMed: 9950759]
122. Yamamoto H, Kawamata T, Ninomiya T, Omote K, Namiki A. Endothelin-1 enhances capsaicin-evoked intracellular Ca^{2+} response via activation of endothelin a receptor in a protein kinase Cε-dependent manner in dorsal root ganglion neurons. Neuroscience. 2006; 137:949–960. [PubMed: 16298080]
123. Wang L, Fortune B, Cull G, Dong J, Cioffi GA. Endothelin B receptor in human glaucoma and experimentally induced optic nerve damage. Arch Ophthalmol. 2006; 124:717–724. [PubMed: 16682595]
124. Lau J, Dang M, Hockmann K, Ball AK. Effects of acute delivery of endothelin-1 on retinal ganglion cell loss in the rat. Exp Eye Res. 2006; 82:132–145. [PubMed: 16045909]

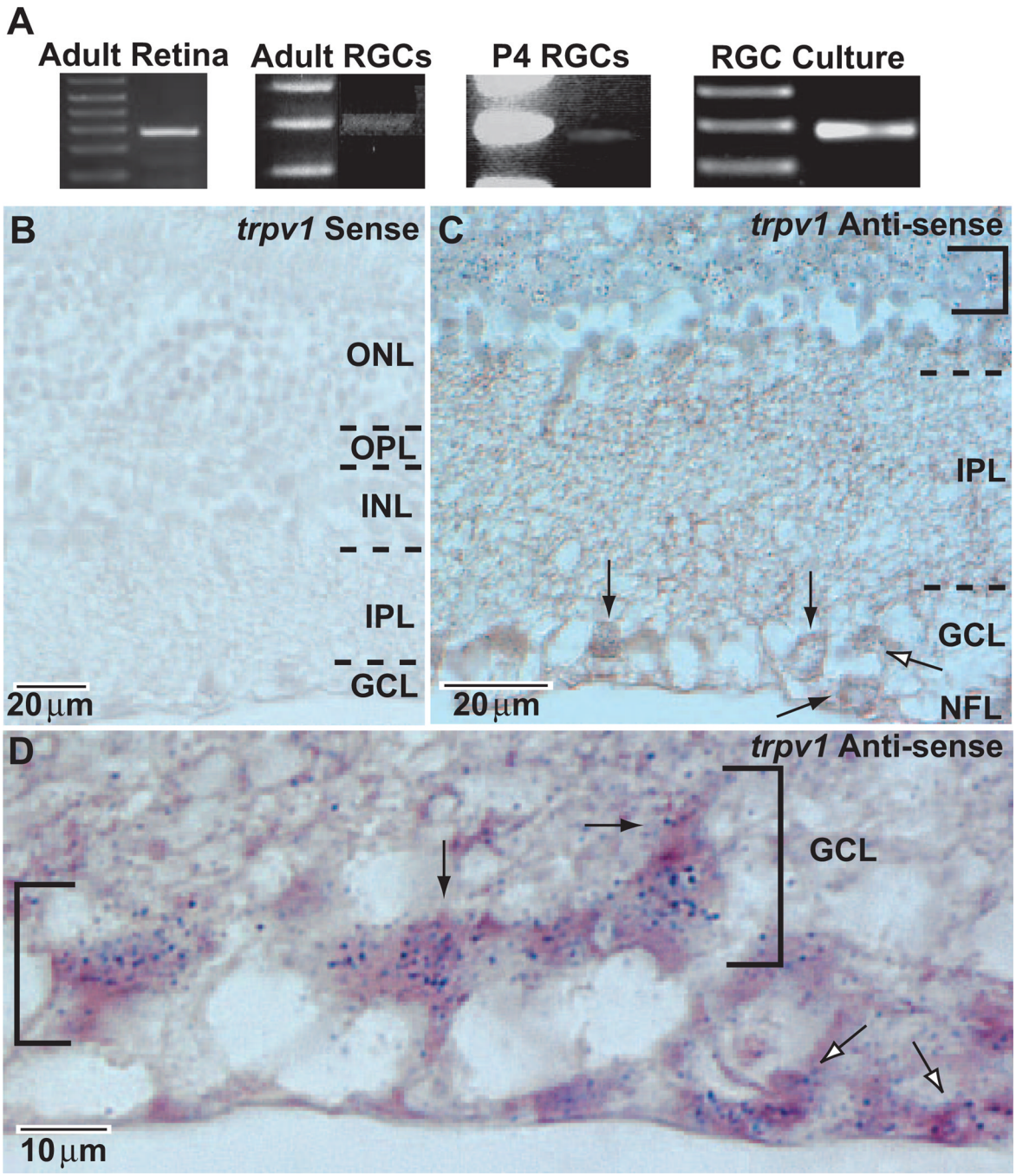

Figure 1.

Expression of *trpv1* mRNA in RGCs. (**A**) PCR demonstrates expression of *trpV1* mRNA in whole retina from adult rat, RGCs isolated from adult and P4 rat retina, and P3 RGCs cultured for 7 days. (**B**) Control in situ hybridization with sense *trpv1* probe reveals little or no background staining. (**C**) Antisense *trpv1* probe strongly labels cell bodies in the middle tier of the INL (*bracket*) and in the GCL of the rat retina. Large cell bodies of RGCs are indicated (*filled arrows*), as is a smaller cell body likely corresponding to a microglial cell (*white arrow*). (**D**) Higher magnification illustrates robust *trpv1* expression in the large cell bodies of RGCs (*filled arrows*) in the GCL and in smaller glial cell bodies in the NFL below

(*white arrows*). ONL, outer nuclear layer; OPL, outer plexiform layer; INL, inner nuclear layer; IPL, inner plexiform layer; GCL, ganglion cell layer; NFL, nerve fiber layer.

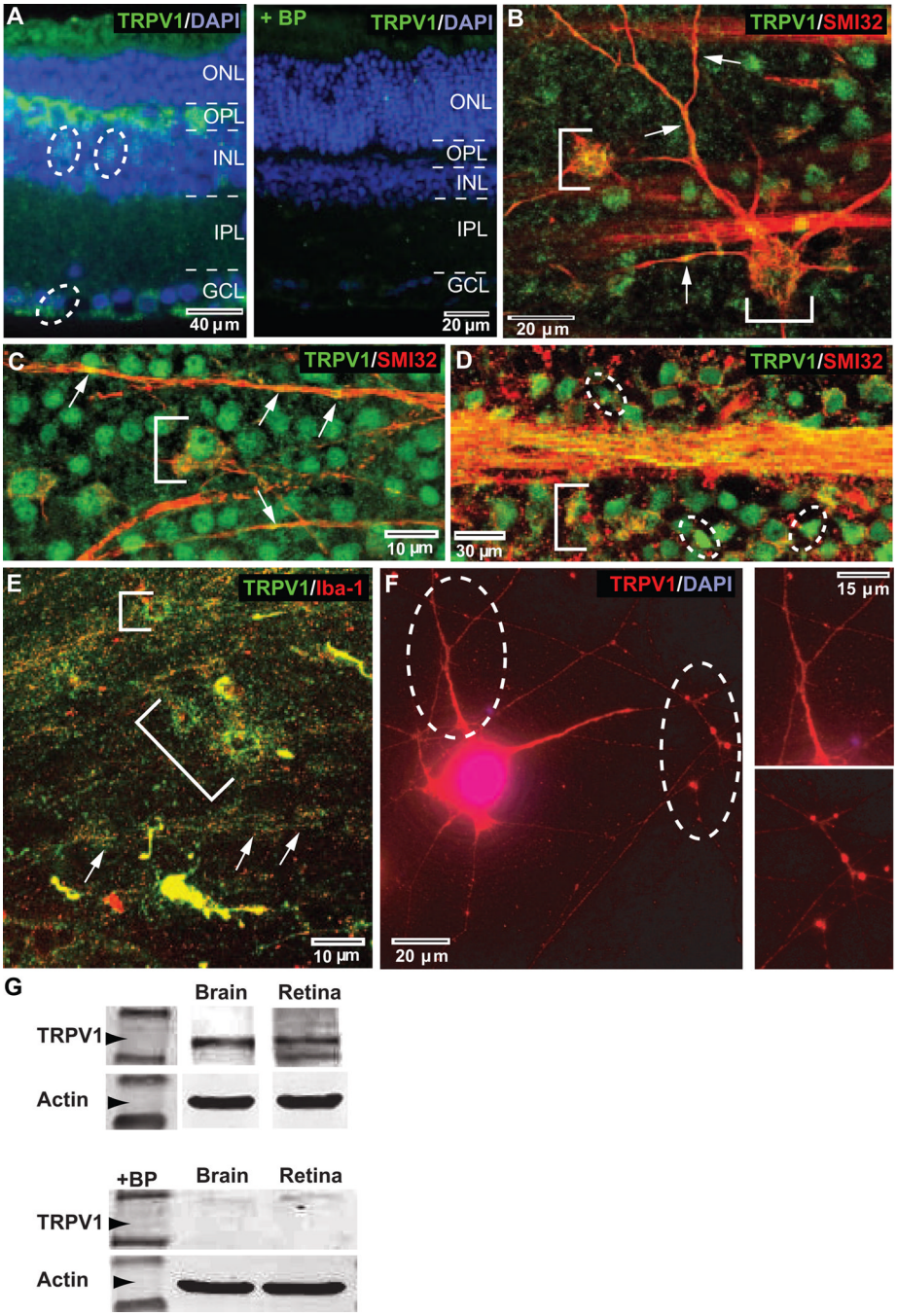

Figure 2.

TRPV1 localization in RGCs of rat retina. (**A**) Immunocytochemical labeling for TRPV1 shows strong localization in the outer retina and in RGCs (large cell bodies); there is little or no label in smaller displaced amacrine cells of the GCL. Clear examples of amoeboid-shaped cell bodies of microglia cells are indicated (*ovals*). *Right*: Control section preabsorbed using the TRPV1 blocking peptide (+BP). (**B**) Confocal image stack through GCL and NFL showing labeling for TRPV1 in wholemount preparation counterlabeled with antibodies against heavy-chain neurofilaments that recognize broad-field RGCs (SMI32). Image shows punctate localization to dendrites (*arrows*) as well as intense label to cell

bodies (*brackets*); smaller cell bodies with TRPV1 label are in the background. (**C**) Confocal image stack through GCL and NFL of peripheral retina shows TRPV1 in RGC cell bodies (*bracket*) and in small bundles of RGC axons (*arrows*). (**D**) Confocal stack from central retina shows TRPV1 in RGC cell bodies (*bracket*) and in axon bundles in the NFL as they course toward the optic nerve head. Amoeboid-shaped cell bodies of microglia are apparent (*ovals*). (**E**) Confocal image in single plane at GCL/NFL border shows Iba-1–labeled microglia processes colocalizing with TRPV1, as we previously demonstrated.[51] TRPV1-label RGC cell bodies (*brackets*) and axons (*arrows*) are indicated for reference. (**F**) Immunocytochemical labeling demonstrates strong perinuclear and dendritic localization of TRPV1 in cultured RGCs counterstained with the nuclear label DAPI. Localization to dendritic processes and neurites (*dashed circles*) includes node-like clusters; *right*: these regions are shown at higher magnification. (**G**, *top*) Western blot against TRPV1 in brain and whole retina from adult rat shows band at expected molecular weight (*arrowheads*; 100 – 113 kDa). Retina demonstrates an additional band with a slightly lower molecular weight that probably corresponds to a different glycosylation state for this antibody.[79] *Bottom*: Control Western blot with preabsorption of TRPV1 antibody using the blocking peptide prevents detection of both bands. ONL, outer nuclear layer; OPL, outer plexiform layer; INL, inner nuclear layer; IPL, inner plexiform layer; GCL, ganglion cell layer; NFL, nerve fiber layer.

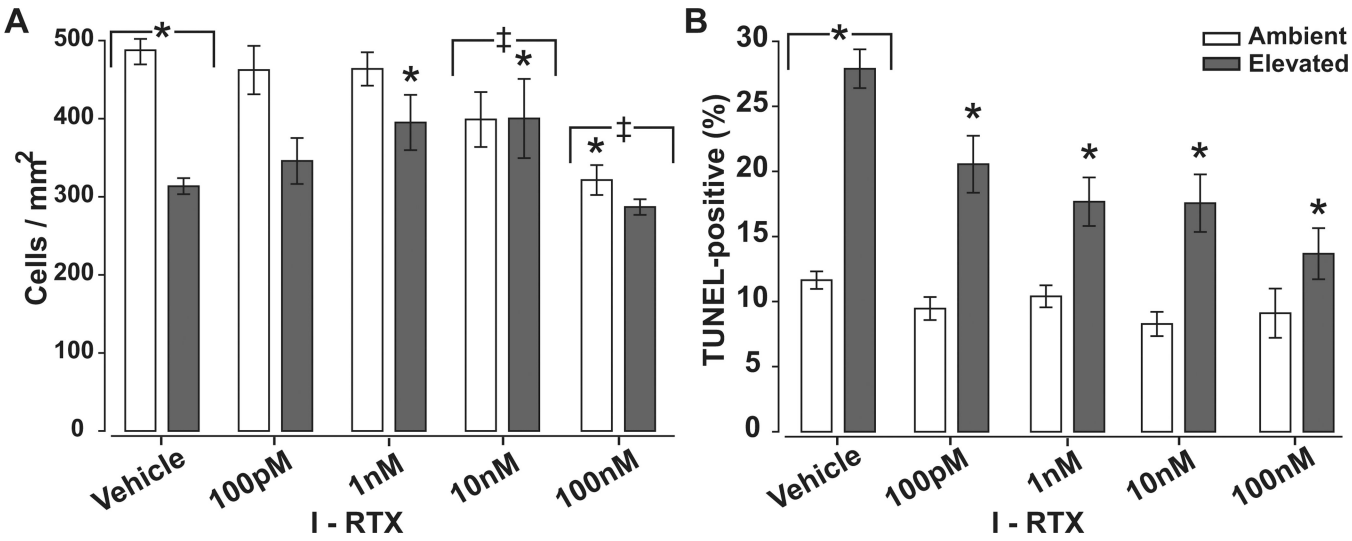

Figure 3.

Antagonism of TRPV1 diminishes pressure-induced RGC apoptosis. (**A**) Density and (**B**) percentage of TUNEL-positive RGCs at ambient or elevated pressure for 48 hours exposed to increasing concentrations of I-RTX. (**A**) For vehicle only, elevated pressure reduces the density of RGCs by 36% compared with ambient pressure (*bracketed* *). Treatment with 1 nM and 10 nM I-RTX increases the density of RGCs at elevated pressure by 20% and 25%, respectively, compared with vehicle alone (*); with 10 nM I-RTX, density for elevated pressure is equivalent to ambient (*bracketed* ‡). Increasing IRTX to 100 nM reduces RGC density at ambient pressure by 35% compared with vehicle alone (*) and at elevated pressure so that the densities are equivalent (*bracketed* ‡). (**B**) For vehicle only, elevated pressure increases the percentage of TUNEL-positive RGCs by nearly 2.5-fold compared with ambient (*bracketed* *). At ambient pressure, treatment with I-RTX does not significantly alter the percentage of TUNEL-positive RGCs compared with vehicle only. For RGCs at elevated pressure, I-RTX steadily decreases the percentage of TUNEL-positive RGCs from 26% for 100 pM to 51%for 100 nM compared with vehicle only (*). *$P \leq 0.05$ (significance); ‡$P \geq 0.1$ (no significance). Error bars represent SEM.

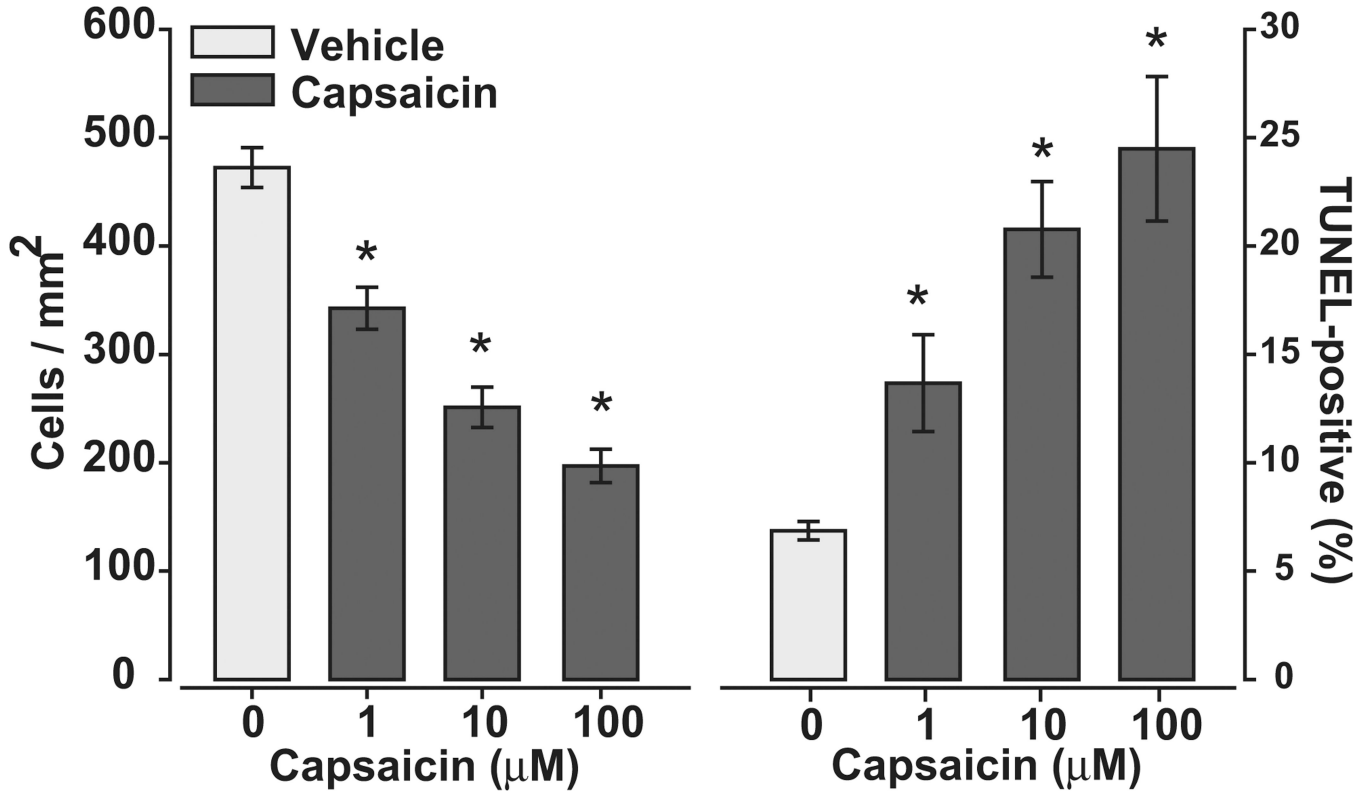

Figure 4.

Activation of TRPV1 induces RGC apoptosis. Density and percentage of TUNEL-positive RGCs in primary cultures exposed to varying concentrations of the TRPV1 agonist capsaicin (1–100 μM) for 48 hours. As capsaicin concentration increases, RGC density decreases and the percentage of TUNEL-positive cells increases. The largest dose of capsaicin decreases RGC density by 58% while increasing the percentage of TUNEL-positive RGCs by 3.5-fold. *$P \leq 0.01$ compared with no treatment. Error bars represent SEM.

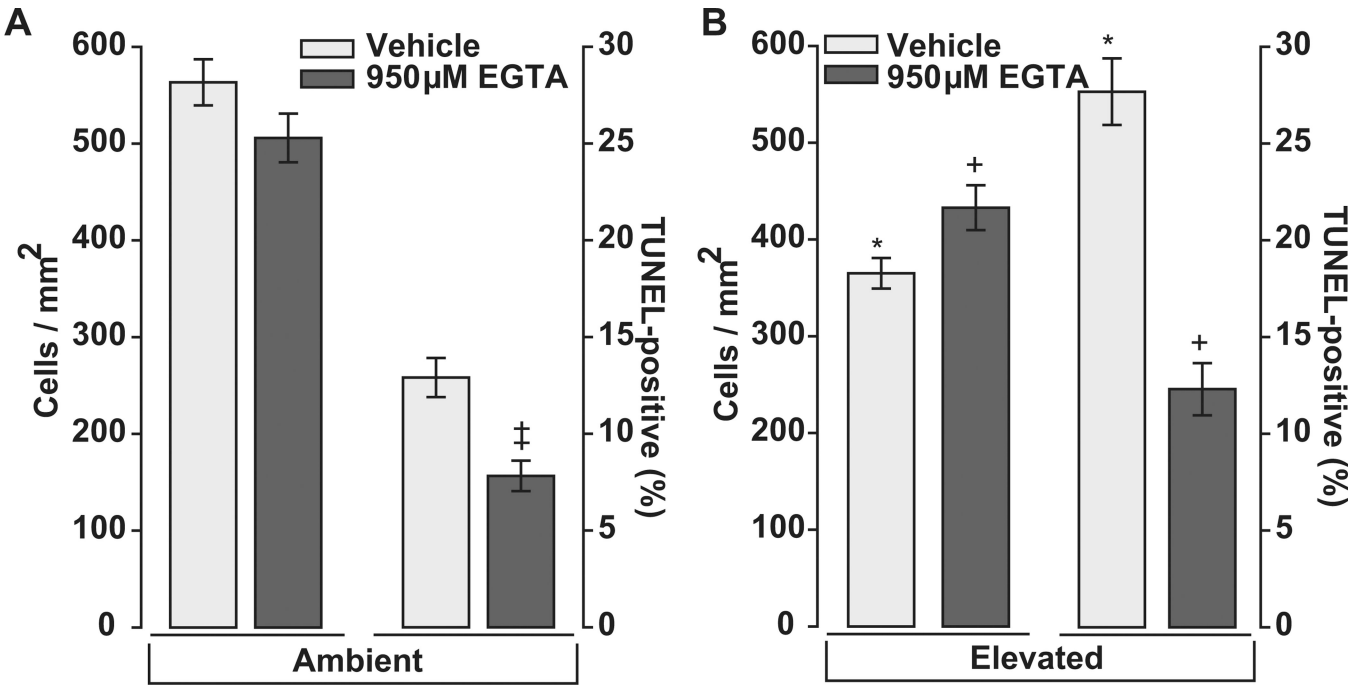

Figure 5.

Chelation of extracellular Ca^{2+} reduces pressure-induced RGC apoptosis. Density and percentage of TUNEL-positive RGCs in primary RGC cultures maintained at ambient (**A**) or elevated (**B**) pressure for 48 hours and treated with 950 μM EGTA. (**A**) Treatment with EGTA does not significantly alter the density of RGCs. However, EGTA does decrease the percentage of TUNEL-positive RGCs by 38% compared with vehicle-treated (‡). (**B**) As in Figure 3, elevated pressure without treatment induces a significant 35% decrease in RGC density compared with ambient pressure (*). This corresponds with a twofold increase in the percentage of TUNEL-positive RGCs (*). Treatment with EGTA modestly increases the density of RGCs by 18% (+), while reducing the percentage of TUNEL-positive RGCs by 56% (+). Symbols indicate $P \leq 0.01$; error bars represent SEM.

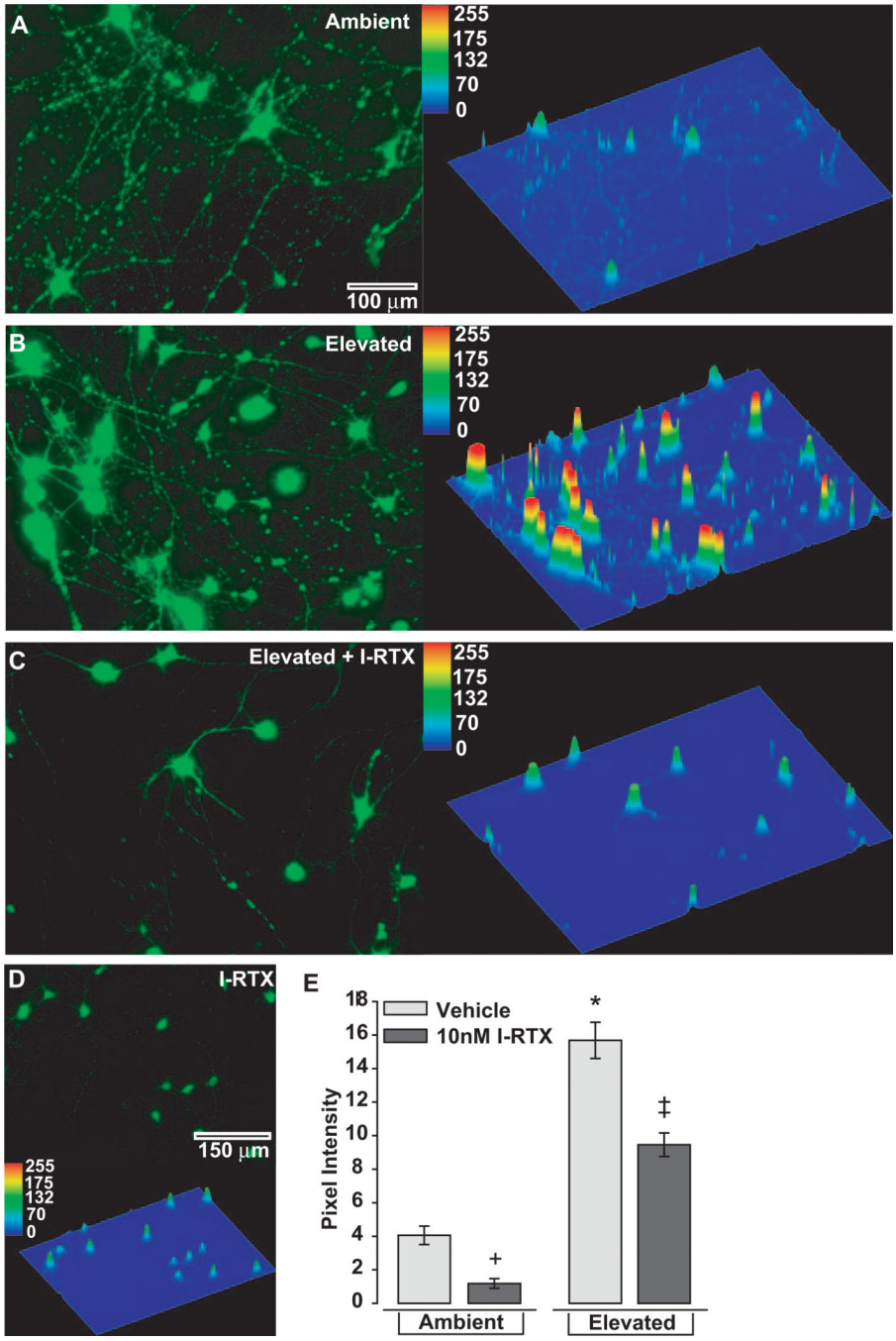

Figure 6.

TRPV1 contributes to pressure-induced increases in RGC Ca^{2+}. (**A**) Fluo-4 conjugated Ca^{2+} accumulation in RGCs at ambient pressure (*left*) and quantification with intensity map (*right*). (**B**) One hour of elevated hydrostatic pressure induces increased intracellular Ca^{2+} in cell bodies and neurites. (**C**) Treatment of RGCs exposed to elevated pressure for 1 hour with 10 nM I-RTX greatly diminishes the Ca^{2+} signal, especially in processes in which Fluo-4 label is almost absent. (**D**) Treatment with 10 nM I-RTX at ambient pressure decreases baseline intracellular Ca^{2+}. (**E**) Quantification of Fluo-4 indicates that elevated pressure induces a significant, fourfold increase from ambient pressure in accumulated

intracellular Ca^{2+} after 1-hour exposure (*). I-RTX treatment significantly reduces ambient (+) and pressure-induced Ca^{2+} (‡). Symbols indicate $P \leq 0.05$; error bars represent SE. Pixel intensity calculated as average of total intensity from 15 to 20 independent fields. Scale bar in (**D**) also applies to (**A–C**).

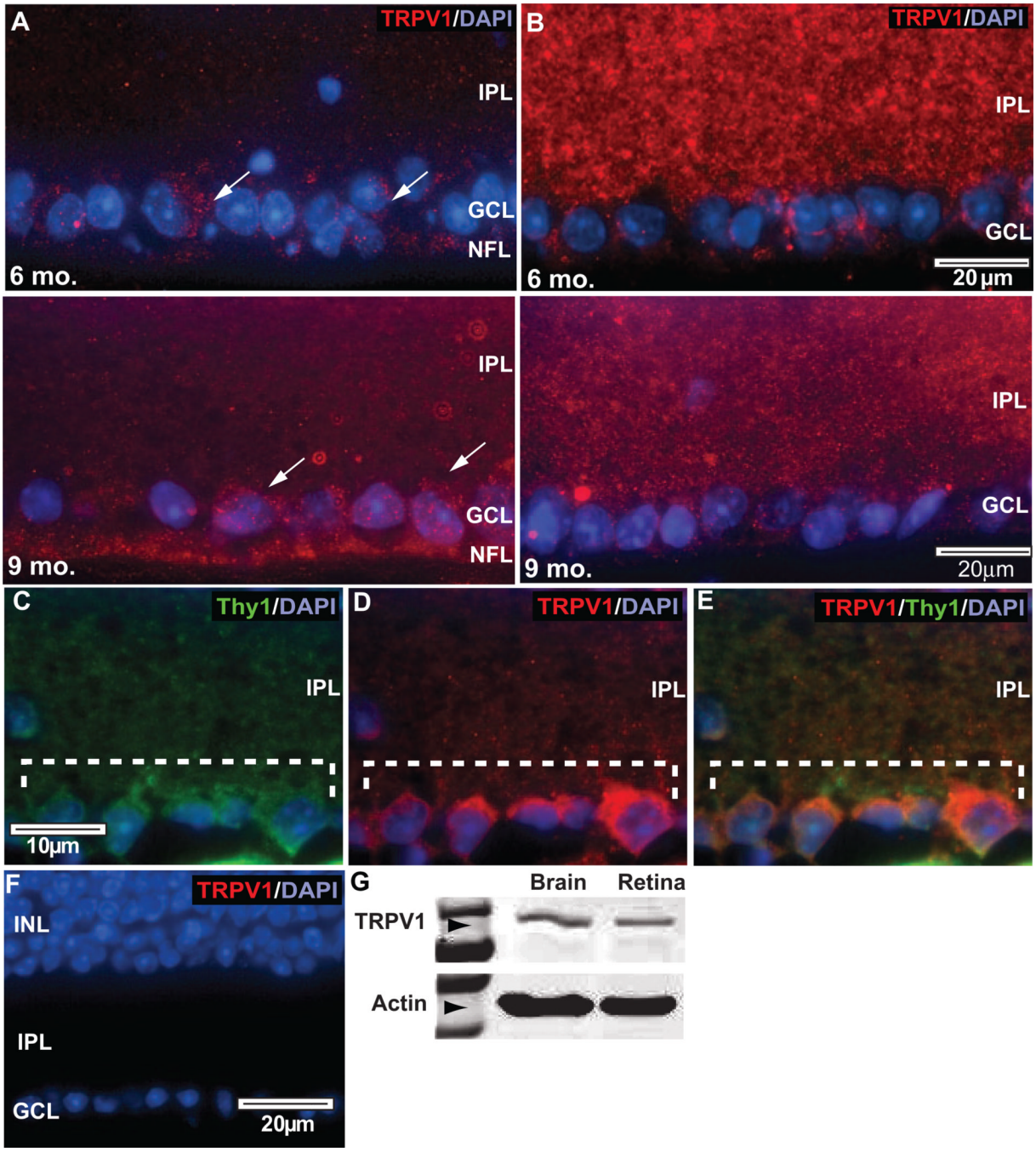

Figure 7.

Elevated IOP increases TRPV1 in DBA/2 mice. Immunolabeling against TRPV1 with DAPI counterstain in retina from DBA/2 mice (**A, B**) and colabeling of the RGC-specific marker Thy1 and TRPV1 C57 retina for comparison (**C–E**). All micrographs from the high RGC density region proximal to the nerve head. (**A**) Retina from 6-month (*top*) and 9-month (*bottom*) DBA/2 eyes with relatively low IOP (average, 14.85 mm Hg for 6 months and 18.5 mm Hg for 9 months) reveals punctate labeling of TRPV1 in the GCL (*arrows*), including the large cell bodies of RGCs. The 9-month retina also demonstrated stronger label in the NFL. (**B**) In retina from 6-month and 9-month DBA/2 eyes with higher IOP for each age

(average, 17.7 mm Hg for 6 months and 21.8 mm Hg for 9 months), TRPV1 label remains strong in the GCL (*bracket*) but also increases dramatically in the IPL. (**C**) The GCL (*dotted bracket*) of C57 retina shows the RGC-specific marker Thy1 highlighting RGC cell bodies (with DAPI counterstain), with lighter labeling in RGC dendrites in the IPL. (**D**) Same field as in (**C**) showing a similar pattern for TRPV1 in RGCs. TRPV1 label appears to be perinuclear and membrane bound in GCL. Lighter TRPV1 labeling is also present in the IPL. (**E**) Merged image of Thy1 (**C**) and TRPV1 labeling (**D**) with DAPI counterstain reveals colocalization. (**F**) C57 section with primary antibody omitted for control. (**G**, *top*) Western blot against TRPV1 and actin in brain and whole retina from adult C57 mouse. Single bands are present at the expected molecular weights for TRPV1 and actin (*arrowheads*). IPL, inner plexiform layer; GCL, ganglion cell layer; NFL, nerve fiber layer.